Structural, electronic, optical and elastic properties of perovskite materials $NaMCl_3$ (M = In, Al): First principle investigations

Roll: 161322

Session: 2016-17

Report submitted to the Department of Physics at
Jashore University of Science and Technology
in partial fulfillment of the requirements
for the degree of Bachelor of Science
with Honours in Physics

January 2022

Abstract

In this report, we studied the structural, electronic, optical, and elastic properties of the metal halide perovskites $NaMCl_3$ (M = In, Al) compounds to investigate their potential as future photovoltaic materials by using the Perdew-Burke-Ernzerhof Generalized Gradient exchange and correlation potential as implemented in WIEN2k code. The electronic band structure showed that our studied compounds are metallic with zero band gap. The optical and elastic properties also confirm the metallic properties of $NaMCl_3$ (M = In, Al) materials. So from the electronic, optical, and elastic properties, we can say that these perovskite compounds can be used as a good metallic conductor.

Acknowledgments

Firstly, I praise and thank Almighty God, the Lords of the worlds, the owner of life and death.

Secondly, I would like to thank my respected supervisor, Dr. Mohammad Abdur Rashid, Assistant Professor, Department of Physics, Jashore University of Science Technology, for his constant support and guidance to complete my project work properly.

I am thankful to the authors of different publications (included in the bibliography), from where I have collected many supplementary pieces of information. Also, my gratitude goes to all faculty members of the department of physics for much helpful decision making at different times.

My appreciation goes to my parents, siblings, and all family members for their prayers, financial and emotional support. Also, my gratitude goes to all faculty members of the department of physics for much helpful decision-making at different times.

I would also like to thank my friends who have helped me to complete this project.

Dedication

This work is dedicated to my family for their relentless support throughout the struggle.

And to all the scientists that keep working to make the world a better place.

Table of Contents

List of Abbreviation

Density-Functional Theory	DFT
Exchange-Correlation	XC
Gradient-Expansion Approximation	GEA
Generalized-Gradient Approximation	GGA
Hartree-Fock	HF
Hohenberg-Kohn	HK
Kohn-Sham	HS
Local Density Approximation	LDA
Perdew-Burke-Ernzerhof	PBE
Photovoltaics	PV
Thomas-Fermi	TF
Self-Consistent Field	SCF
Electron Energy Loss	EEL

List of Figures

List of Tables

Structural, electronic, optical and elastic properties of perovskite materials $NaMCl_3$ (M = In, Al): First principle investigations

Chapter 1

Introduction

The name of the systems we studied are $NaMCl_3$ (M = In, Al). These materials are called metal halide perovskite materials. The most well-known forms of perovskite crystals found on Earth are halide-perovskites (ABX_3), oxide-perovskites (ABO_3), and nitride-perovskites (ABN_3). Halide perovskites have attracted a lot of interest as a result of their widespread use in the optical, energy storage, and semiconducting industries [1]. Perovskites $NaMCl_3$ (M = In, Al) have cubic structures (space group Pm-3m). The general chemical formula used to describe the halide perovskite materials is ABX_3, where A and B are cations with A being bigger than B and X being the anion, which is commonly oxides or halogens [2]. The perovskite crystal family covers a wide range of physical properties, including high magneto resistance, a low-temperature coefficient of resistivity, and laser sources. Depending on their chemical compositions and elemental configurations, perovskites exhibit a wide variety of physical characteristics [3–5]. In $NaMCl_3$ (M = In, Al) compounds Na is a monovalent cation, Al and In are trivalent metal cations and Cl is a halogen group atom. In this manuscript, we calculated the structural, electronic, optical, and elastic properties of $NaMCl_3$ (M = In, Al) compounds to highlight their potential in future photovoltaic applications [6].

Significant growth in energy use, as well as other serious environmental challenges linked with traditional sources, has sounded the alarm for the scientific community to look for long-term sustainable alternatives. Renewable energy sources are often regarded as the most convenient

and hassle-free option, and solar energy is unanimously regarded as the most dominating non-conventional source for desired energy production. Solar cells, which are used to gather solar energy, play an important part in achieving efficient energy production. Among all preceding estimates, developing unique solar materials with properties such as cheaper cost, efficient generating capacity, eco-friendly nature, and universal compatibility is a top priority [7,8]. Perovskites halides are being studied extensively because of their intriguing and enticing features, as well as their wide range of uses and availability as a common mineral on Earth[9]. Ferro electricity, charge ordering, superconductivity, gigantic magneto resistance, high thermo power, spin-dependent transport, and exotic structural, electrical, magnetic, optical, and transport properties are among the characteristics discovered. They are also regarded as prospective materials for microelectronics and telecommunications due to their promise in a variety of technical applications such as fuel cells, sensors, memory devices, spintronics, and photovoltaics [10–12]. Different kinds of perovskite materials were researched extensively, including chalcogenide perovskite (AMO_3) and halide perovskite (ABX_3), which is classed as alkali halide and organometal halide. Oxide-based perovskites have been intensively explored for their excellent ferroelectric and superconducting characteristics in a variety of applications. The most widely used metal halide perovskites are cesium lead halide ($CsPbX_3$) and methylammonium lead halide ($CH_3NH_3PbX_3$) perovskites [2]. The halide perovskites, particularly lead-based perovskites, have high power conversion efficiencies and may thus be used in a variety of optoelectronics applications including photovoltaics, light-emitting diodes, sensors, lasers, and radiation detectors. The poisonous nature of lead, which is exceedingly harmful to mental development, human growth, and the entire environment, is the primary disadvantage of these lead-based perovskites [13]. We studied $NaMCl_3$ (M=In, Al) materials because these materials' structural, electronics, optical and chemical properties are unknown and these materials are not harmful to human health. Perovskite material's distinctive physical features, such as high absorption coefficient, long-range ambipolar charge transfer, low exciton-binding energy, high dielectric constant, ferroelectric properties, and so on, have attracted a lot of interest in optoelectronic and photovoltaic applications [2].

The structural, electrical, and optical characteristics of lead-free tin halide perovskite $NaMCl_3$ (M = In, Al) compounds are calculated using the WIEN2k code and the full potential linearized augmented plane wave (FP-LAPW) method[14]. It's worth noting that the solution to the well-known Kohn-Sham equation for a periodic crystal system is provided in this manner [15].

$$\psi_k = \sum_n c_n \varphi_{k_n}$$

Here, ψ_k is the wave function, k_n is the reciprocal lattice vector and c_n represents the coefficient of the Rayleigh-Ritz vibrational principle respectively. It's also worth noting that the correctness of the results is determined by the exchange-correlation functional used[15]. The Perdew-Burke-Ernzerhof Generalized-Gradient-Approximation (PBE-GGA) is used in the current computations [16].

WIEN2k is a Fortran-based computer application that conducts quantum mechanical computations on periodic solids. It solves the Kohn–Sham equations of density functional theory using the full-potential (linearized) augmented plane-wave and local-orbitals [FP-LAPW + lo] basis set. WIEN2k calculates a solid's electrical structure using density functional theory. It is based on the full potential energy (linear) augmented plane wave ((L) APW) + local orbit (lo) approach, which is the most precise way for calculating the bond structure. In density universal information, local (spin) density approximation (LDA) or generalized gradient approximation (GGA) can be utilized [14]. It is considered to be one of the most accurate solid modeling approaches.

In this project, we begin with the introduction of metal perovskite $NaMCl_3$ (M = In, Al) materials in the first chapter. In this chapter, we have discussed what is $NaMCl_3$ (M = In, Al) materials, what is its importance, and why we are studying it. In chapter 2 we discuss the basic quantum mechanics which starts with Schrodinger's groundbreaking equation. This chapter contains time-independent equations, wave function, Born-Oppenheimer approximation, the Hartree-Fock approach, and the limitations of the Hartree-Fock approach. Chapter 3 contains the theoretical investigation of Density Functional Theory (DFT). In this chapter, we discussed the electron density, Thomas-Fermi theory, Hohenberg-Kohn theory, Kohn-Sham equations, Solving the Khon-Sham equation, and the Exchange-correlation potential such as Local density approximation (LDA), Hybrid functional approach, Generalized-Gradient Approximation (GGA). In chapter 4, we presented the results and discussions part of this project. In this chapter, firstly we find the crystal structure then we calculate the energy band structure, the density of states (DOS), optical absorption, conductivity, reflectivity, refractivity, real and imaginary dielectric tensor, and elastic properties of $NaInCl_3$ and $NaAlCl_3$. We have also done the non-magnetic volume optimization and SCF calculation of perovskite $NaMCl_3$ (M = In, Al) materials. And in chapter 5 we discussed the overall conclusion of this report.

Chapter 2

Basic Quantum Mechanics

2.1 Schrodinger groundbreaking equation

In 1926, Erwin Schrödinger attempt to describe the so-called ‘matter waves’, where he used de Broglie’s relations to describe hypothetical plane waves, led to the most general form of the equation named after him, the time-dependent Schrodinger equation [17]

$$\mathrm{i}\hbar\frac{\partial}{\partial t}\psi(\vec{r},\, t) = \hat{H}\psi(\vec{r},\, t). \tag{2.1}$$

Because a fully relativistic formulation of the formula is frequently impractical, Schrödinger proposed a non-relativistic approximation, which is now widely employed, particularly in quantum chemistry.

Using the Hamiltonian for a single particle

$$\hat{H} = \hat{T} + \hat{V} = -\frac{\hbar^2}{2m}\vec{\nabla}^2 + V\,(\vec{r},\, t) \tag{2.2}$$

leads to the (non-relativistic) time-dependent single-particle Schrödinger equation

$$i\hbar\frac{\partial}{\partial t}\psi\,(\vec{r},\, t) = [-\frac{\hbar^2}{2m}\vec{\nabla}^2 + V(\vec{r},\, t)\,]\,\hat{H}\psi\,(\vec{r},\, t). \tag{2.3}$$

In this project, from now on only non-relativistic cases are considered.

For N particles in three dimensions, the Hamiltonian is

$$\hat{H} = \sum_{i=1}^{N} -\frac{\hat{p}_i{}^2}{2m_i} + V(\vec{r}_1, \vec{r}_2 \ldots, \vec{r}_N, t) = -\frac{\hbar^2}{2}\sum_{i=1}^{N}\frac{1}{m_i} + V(\vec{r}_1, \vec{r}_2 \ldots, \vec{r}_N, t). \quad (2.4)$$

The corresponding Schrödinger equation reads

$$i\hbar\frac{\partial}{\partial t}\psi(\vec{r}_1, \vec{r}_2 \ldots, \vec{r}_N, t) = [-\frac{\hbar^2}{2}\sum_{i=1}^{N}\frac{1}{m_i}\nabla_i{}^2 + V(\vec{r}_1, \vec{r}_2 \ldots, \vec{r}_N, t)]\,\psi(\vec{r}_1, \vec{r}_2 \ldots, \vec{r}_N, t) \quad (2.5)$$

2.2. Time-independent equation

The solutions of the time-independent Schrödinger equation, where the Hamiltonian has no time dependence (implying a time-independent potential), are special instances. The solutions to the time-independent Schrödinger equation are special examples, where the Hamiltonian itself has no time-dependency (which implies a time-independent potential $V(\vec{r}_1,\vec{r}_2 \ldots, \vec{r}_N, t)$, and the solutions, therefore, illustrate standing waves which are called stationary states or orbitals). The time-independent Schrödinger equation is not only easier to deal with, but understanding its solutions also gives essential insight into dealing with the equivalent time-dependent equation, and the solutions, therefore, characterize stationary states or orbitals). The time-independent Schrödinger equation is not only simpler to solve, but understanding its solutions also gives you valuable insight into how to solve the time-dependent Schrödinger equation.

The separation of variables technique is used to create the time-independent equation, in which the spatial portion of the wave function is separated from the temporal part via the spatial part of the wave function [18].

$$\psi(\vec{r}_1, \vec{r}_2 \ldots, \vec{r}_N, t) = \psi(\vec{r}_1, \vec{r}_2, \ldots, \vec{r}_N)\ \tau(t) = \psi(\vec{r}_1, \vec{r}_2, \ldots, \vec{r}_N).\, e^{-i\omega t} \quad (2.6)$$

In addition, the l.h.s. of the equation simplifies to the Hamiltonian's energy eigenvalue multiplied by the wave function, yielding the general eigenvalue equation

$$E\psi(\vec{r}_1, \vec{r}_2, \ldots, \vec{r}_N) = \hat{H}\psi(\vec{r}_1, \vec{r}_2, \ldots, \vec{r}_N) \quad (2.7)$$

The Schrödinger equation is rewritten using the many-body Hamiltonian once again

$$E\psi(\vec{r}_1, \vec{r}_2, \ldots, \vec{r}_N) = [-\frac{\hbar^2}{2}\sum_{i=1}^{N}\frac{1}{m_i}\nabla_i{}^2 + V(\vec{r}_1, \vec{r}_2, \ldots, \vec{r}_N]\,\psi(\vec{r}_1, \vec{r}_2, \ldots, \vec{r}_N). \quad (2.8)$$

2.3 The Wave Function

In quantum physics, a wave function is a mathematical representation of the quantum state of an isolated quantum system. The wave function is a complex-valued probability amplitude from which probabilities for the potential outcomes of system observations may be calculated. The Greek letters ψ and Ψ are the most used symbols for wave functions (lower-case and capital psi, respectively).

The first and most essential postulate is that a particle's state is fully represented by its (time-dependent) wave function, which means that the wave function includes all information about the particle's state.

The discussion will be limited to the time-independent wave function for simplicity. When it comes to physical quantities, there's always the subject of possible interpretations as well as observations. A basic premise of the Copenhagen interpretation of quantum mechanics is the Born probability interpretation of the wave function, which offers a physical explanation for the square of the wave function as a probability density [19,20]

$$|\psi(\vec{r}_1, \vec{r}_2 \ldots., \vec{r}_N)|^2 \, d\vec{r}_1 d\vec{r}_2 \ldots. d\vec{r}_N. \tag{2.9}$$

The chance of particles 1,2,...,N being found in the same volume element $d\vec{r}_1 d\vec{r}_2 \ldots. d\vec{r}_N$ at the same time is described by equation (2.9) [21]. It's also important to think about what occurs if two particles' locations are switched. The overall probability density cannot rely on such an interchange, i.e.

$$|\psi(\vec{r}_1, \vec{r}_2 \ldots., \vec{r}_i, \vec{r}_j, .., \vec{r}_N)|^2 = |\psi(\vec{r}_1, \vec{r}_2 \ldots., \vec{r}_j, \vec{r}_i, .., \vec{r}_N)|^2 \tag{2.10}$$

During a particle exchange, there are only two possible outcomes for the wave function. The first is a symmetrical wave function that remains unchanged as a result of the exchange. This is what bosons are like (particles with integer or zero spins). Another alternative is an anti-symmetrical wave function, in which a sign change occurs when two particles are exchanged, which corresponds to fermions (particles with half-integer spin) [22,23].

Only electrons, which are fermions, are discussed in this report. The Pauli principle asserts that no two electrons may be in the same state, where state refers to the wave function's orbital and spin parts (the term spin coordinates will be discussed later in more detail). The antisymmetry principle is a quantum-mechanical formalization of Pauli's theoretical theories in spectrum description (e.g. alkaline doublets) [22,23].

The normalizing of the wave function is another consequence of the probability interpretation. If equation (2.9) explains the chance of finding a particle in a volume element, using the whole range of coordinates as the volume element must provide a probability of one, implying that all particles must be located someplace in space. This is the same as the wave function's normalizing criterion.

$$\int d\vec{r}_1 \int d\vec{r}_2 \ldots \int d\vec{r}_N \, |\psi(\vec{r}_1, \vec{r}_2 \ldots\ldots, \vec{r}_j, \vec{r}_i, .., \vec{r}_N)|^2 = 1 \qquad (2.11)$$

Equation (2.11) also reveals the physical conditions that a wave function must meet. Wave functions must be square-integrable and continuous over the whole spatial range.

Another essential aspect of the wave function is that computing the expectation values of operators with it yields the expectation value of the corresponding observable. For an observable $O(\vec{r}_1, \vec{r}_2 \ldots\ldots, \vec{r}_N)$, this can generally be written as

$$O = \langle O \rangle = \int d\vec{r}_1 \int d\vec{r}_2 \ldots \int d\vec{r}_N \, \psi^* (\vec{r}_1, \vec{r}_2 \ldots\ldots, \vec{r}_N) \hat{O} \, \psi (\vec{r}_1, \vec{r}_2 \ldots\ldots, \vec{r}_N). \qquad (2.12)$$

2.4 Born-Oppenheimer approximation

Because nuclei are substantially heavier than electrons, the adiabatic or Born-Oppenheimer (B-O) approximation is based on the fact that electron velocities are much greater than nuclei speeds (Born & Oppenheimer, 1927). In the Born-Oppenheimer approximation, we freeze the nuclear position and calculate the electronic wave function and energy

$$\hat{H}_{B-O}(R) = -\frac{1}{2}\sum_i \nabla_i^2 - \sum_{i,I} \frac{Z_I}{|r_i - R_I|} + \frac{1}{2}\sum_{i \pm I} \frac{e^2}{|r_i - r_j|} \qquad (2.13)$$

Where the first, second, and third terms are respectively, the kinetic energy of the electrons, the electrons-nucleus Coulomb interaction, and the electron-electron Coulomb interaction. The two-body Coulomb terms and the exchange-correlation (in the third term) in the many-body equation (eqn. 2.13) necessitate additional reduction. This problem may be greatly simplified using Density Functional Theory (DFT) [24].

2.5 The Hartree-Fock approach

The Hartree-Fock (HF) approximation, commonly known as the mean-field approximation (also known as self-consistent field approximation), presents an approximation that allows a physical issue to be solved analytically in some cases. The HF technique is primarily concerned

with numerically addressing difficult many-body issues based on the study of effective non-interacting particle models since it provides valuable insight into the features of many-electron systems. The ansatz used to express a many-body wave function is unique to the HF approach [24].

Variational calculus, which is comparable to the least-action principle of classical mechanics, may be used to find a viable method for approximating the analytically not accessible solutions to many-body problems. The ground state wave function ψ_0 may be approximated via variational calculus and corresponds to the system's lowest energy E_0. T. Flieβbach has offered an excellent source of information on the fundamentals of variational calculus [25].

So, at this moment only the electronic Schrodinger equation is of interest, therefore in the next part we set $\widehat{H} \equiv \widehat{H}_{el}$, $E \equiv E_{el}$, and so on.

The expectation values of operators are used to compute observables in quantum mechanics. Because the Hamilton operator corresponds to the energy as an observable, the energy of a generic Hamiltonian may be computed as [18,20]

$$E = \langle \widehat{H} \rangle = \int d\vec{r}_1 \int d\vec{r}_2 \ldots \int d\vec{r}_N \, \psi^* (\vec{r}_1, \vec{r}_2 \ldots, \vec{r}_N) \widehat{H} \, \psi (\vec{r}_1, \vec{r}_2 \ldots, \vec{r}_N). \qquad (2.14)$$

According to the Hartree-Fock method, the energy acquired by any (normalized) trial wave function that differs from the real ground state wave function is always an upper bound, i.e. larger than the actual ground state energy. If the trial function occurs to be desired ground state wave function, the energies are equal

$$E_{trial} \geq E_0 \qquad (2.15)$$

With

$$E_{trial} = \int d\vec{r}_1 \int d\vec{r}_2 \ldots \int d\vec{r}_N \, \psi^*_{trial} (\vec{r}_1, \vec{r}_2 \ldots, \vec{r}_N) \widehat{H} \, \psi_{trial} (\vec{r}_1, \vec{r}_2 \ldots, \vec{r}_N). \qquad (2.16)$$

and

$$E_0 = \int d\vec{r}_1 \int d\vec{r}_2 \ldots \int d\vec{r}_N \, \psi^*_0 (\vec{r}_1, \vec{r}_2 \ldots, \vec{r}_N) \widehat{H} \, \psi_0 (\vec{r}_1, \vec{r}_2 \ldots, \vec{r}_N). \qquad (2.17)$$

According to the Hartree-Fock method, the energy acquired by any (normalized) trial wave function that differs from the real ground state wave function is always an upper bound, i.e. larger than the actual ground-state energy [26].

In that notation, equations (2.15) to (2.18) can be written as

$$\langle \psi_{trial} \,|\widehat{H}|\psi_{trial} \rangle = E_{trial} \;\geq\; E_0 = \langle \psi_0 \,|\widehat{H}|\psi_0 \rangle \tag{2.18}$$

Proof: [20] The eigenfunctions ψ_i of the Hamiltonian $\widehat{H}$ (each corresponding to an energy eigenvalue E_i) form a complete basis set, therefore any normalized trial wave function ψ_{trial} can be expressed as linear combination of those eigenfunctions.

$$\psi_{trial} = \sum_i \lambda_i \psi_i \tag{2.19}$$

The eigenfunctions are assumed to be orthogonal and normalized in this case. As a result of the request to normalize the trial wave function, it follows that

$$\langle \psi_{trial} \,|\psi_{trial} \rangle = \langle \sum_i \lambda_i \psi_i \,|\sum_j \lambda_j \psi_j \rangle = \sum_i \sum_j \lambda_i^{*} \lambda_j \langle \psi_i \,|\psi_j \rangle = |\lambda_j|^2 \tag{2.20}$$

On the other hand, following (2.17) and (2.19)

$$E_{trial} = \langle \psi_{trial} \,|\widehat{H}|\psi_{trial} \rangle = \langle \sum_i \lambda_i \psi_i \,|\widehat{H}|\sum_j \lambda_j \psi_j \rangle = \sum_j E_j \,|\lambda_j|^2 \tag{2.21}$$

In addition, the ground state energy E_0 is the lowest possible energy per definition, and therefore has the smallest eigenvalue ($E_0 \leq E_i$), it is found that

$$E_{trial} = \sum_j E_j \,|\lambda_j|^2 \;\geq\; E_0 \sum_j |\lambda_j|^2 \tag{2.22}$$

what is similar to an equation (2.18)

One of the main concepts of density functional theory is the mathematical framework employed above, i.e. rules that assign numerical values to functions, also known as functional. A function receives a numerical input and produces a numerical output, whereas a functional receives a function and produces a numerical output [27].

Equations (2.14 to 2.22) also contain that a search for the lowest energy value when applied on all allowed N- electron wave functions will always provide the ground-state wave function. Expressed in terms of functional calculus, where $\psi \rightarrow N$ addresses all allowed N-electron wave functions, this indicates [21]

$$E_0 = \min_{\psi \rightarrow N} E[\psi] = \min_{\psi \rightarrow N} \langle \psi | \widehat{H} | \psi \rangle = \min_{\psi \rightarrow N} \langle \psi | \widehat{T} + \widehat{V} + \widehat{U} \,| \psi \rangle. \tag{2.23}$$

Due to the vast number of alternative wave functions on one hand and computer power and time constraints on the other, this search is essentially unfeasible for N-electron systems. What is possible is the restriction of the search to a smaller subset of the possible wave function, as it is done in the Hartree-Fock approximation.

In the Hartree-Fock approach, the search is restricted to approximations of the N-electron wave function by an antisymmetric product of N (normalized) one-electron wave-functions, the so-called spin-orbitals $\chi_i\,(\bar{x}_i\,)$. A wave function of this type is called Slater-determinant and reads [21,28]

$$\psi_0 \;\approx\; \emptyset_{SD} \;= (N!)^{-\frac{1}{2}} \begin{bmatrix} \chi_1(\bar{x}_1\,) & \cdots & \chi_N(\bar{x}_1\,) \\ \vdots & \ddots & \vdots \\ \chi_1(\bar{x}_N\,) & \cdots & \chi_N(\bar{x}_N\,) \end{bmatrix} \tag{2.24}$$

It is important to notice that the spin-orbitals $\chi_i\,(\bar{x}_i\,)$ are not only depending on spatial coordinates but also on a spin coordinate which is introduced by a spin function, $\bar{x}_i \;=\; \bar{r}_i\,, s$.

Returning to the variational principle and equation (2.23), the ground state energy approximated by a single slater determinant becomes

$$E_0 \;= \underset{\emptyset_{SD}\,\to \mathrm{N}}{min} E[\emptyset_{SD}\,] = \underset{\emptyset_{SD}\,\to \mathrm{N}}{min} \langle \emptyset_{SD}\, \big|\widehat{H}\big| \emptyset_{SD}\, \rangle = \underset{\emptyset_{SD}\,\to \mathrm{N}}{min} \langle \emptyset_{SD}\, \big|\widehat{T} \;+\; \widehat{V} \;+\; \widehat{U}\, \big| \emptyset_{SD}\, \rangle \tag{2.25}$$

A general expression for the Hartree-Fock Energy is obtained by usage of the Slater determinant as a trial function

$$E_{HF} \;= \langle \emptyset_{SD}\, \big|\widehat{H}\big| \emptyset_{SD}\, \rangle = \langle \emptyset_{SD}\, \big|\widehat{T} \;+\; \widehat{V} \;+\; \widehat{U}\, \big| \emptyset_{SD}\, \rangle \tag{2.26}$$

For the sake of brevity, a detailed derivation of the final expression for the Hartree-Fock energy is omitted. It is a straightforward calculation found for example in the Book by Schwabl [18].

The final expression for the Hartree-Fock energy contains three major parts: [21]

$$E_{HF} \;= \langle \emptyset_{SD}\, \big|\widehat{H}\big| \emptyset_{SD}\, \rangle = \sum_i^N \langle i \big|\hat{\mathrm{h}}\big| i \rangle + \tfrac{1}{2} \sum_i^N \sum_j^N [\langle ii|jj\rangle - \langle ij|ji\rangle] \tag{2.27}$$

with

$$\langle i \big|\hat{\mathrm{h}}\big| i \rangle = \; \chi^{\,*}{}_i\,(\bar{x}_i\,) \left[-\tfrac{1}{2} \overrightarrow{\nabla_i^2} - \sum_{k=1}^M \frac{Z_k}{r_{ik}} \right] \chi_i\,(\bar{x}_i\,)\, d\bar{x}_i\,, \tag{2.28}$$

$$\langle ii|jj\rangle = \; \iint |\chi_i\,(\bar{x}_i\,)|^2\, \frac{1}{r_{ij}}\, \left|\chi_j(\bar{x}_j)\right|^2\, d\bar{x}_i\, d\bar{x}_j\,, \tag{2.29}$$

$$\langle ii|jj\rangle = \; \iint \chi_i\,(\bar{x}_i\,)\, \chi^{\,*}{}_j(\bar{x}_j\,)\, \frac{1}{r_{ij}}\, \chi_j(\bar{x}_j)\, \chi^{\,*}{}_i\,(\bar{x}_i\,)\, d\bar{x}_i\, d\bar{x}_j \tag{2.30}$$

The first term corresponds to the kinetic energy and the nucleus-electron interactions, ħ denoting the single-particle contribution of the Hamiltonian, whereas the latter two terms

correspond to electron-electron interactions. They are called Coulomb and exchange integral, respectively [21,28].

Examination of equations (2.27) to (2.30) furthermore reveals that the Hartree-Fock energy can be expressed as a function of the spin orbitals $E_{HF} = E[\{\chi_i\}]$. Thus, variation of the spin orbitals leads to the minimum energy [21].

An important point is that the spin orbitals remain orthonormal during minimization. This restriction is accomplished by the introduction of Lagrangian multipliers λ_i in the resulting equations, which represent the Hartree-Fock equations. For a detailed derivation, the reader is referred to the book by Szabo and Ostlund [25].

Finally, one arrives at

$$\hat{f}\chi_i = \lambda_i\chi_i \qquad i = 1,2,\ldots\ldots N \tag{2.31}$$

with

$$\hat{f}_i = -\frac{1}{2}\vec{\nabla}_i^2 - \sum_{k=1}^{M}\frac{Z_k}{r_{ik}} + \sum_i^N\left[\hat{J}_j\vec{x}_i - \hat{K}_j\vec{x}_i\right] = \hat{h}_i + \hat{V}^{HF}(i), \tag{2.32}$$

the Fock operator for the i-th electron. In similarity to (2.27) to (2.30), the first two terms represent the kinetic and potential energy due to nucleus-electron interaction, collected in the core Hamiltonian $\hat{h}_\iota$, whereas the latter terms are sums over the Coulomb operators $\hat{J}_j$ and the exchange operators $\hat{K}_j$with the other j electrons, which form the Hartree-Fock potential $\hat{V}^{HF}$.

There the major approximation of Hartree-Fock can be seen. The two-electron repulsion operator from the original Hamiltonian is exchanged by a one-electron operator $\hat{V}^{HF}$ which describes the repulsion on average. [21]

2.6 Limitations and failings of the Hartree-Fock approach

The number of electrons in an atom or a molecule might be even or odd. The compound is in a singlet state if the number of electrons is even and they are all in double occupied spatial orbitals, $\emptyset_i$. Closed-shell systems are what they're called. Open-shell systems are compounds with an odd number of electrons and compounds with single occupied orbitals, i.e. species with a triplet or higher ground state. These two sorts of systems relate to two different Hartree-Fock techniques. The restricted HF technique (RHF) considers all electrons to be coupled in orbitals,

whereas the unconstrained HF method (UHF) removes this restriction entirely. Open-shell systems may alternatively be described using an RHF method, in which only the single occupied orbitals are eliminated, resulting in a limited open-shell HF (ROHF), which is more realistic but also more difficult and hence less popular than UHF [21].

Closed-shell systems, on the other hand, need an unlimited approach to get good outcomes. For example, a system that places both electrons in the same spatial orbital cannot properly describe the dissociation of H_2 (i.e. the behavior at high internuclear distances), because one electron must be positioned at one hydrogen atom. As a result, in HF calculations, technique selection is always crucial [28].

Kohn states several $M = p^5$ with $3 \leq p \leq 10$ parameters for an output with adequate accuracy in the investigations of the H_2 system [29]. For a system with *N = 100* electrons, the number of parameters rises to

$$M = p^{3N} = 3^{300}\ to\ 10^{300} \approx 10^{150}\ to\ 10^{300} \tag{2.33}$$

According to equation (2.33), energy reduction would have to be done in a space with at least 10^{150} dimensions, which is well above current computer capabilities. As a result, HF methods are limited to situations involving a modest number of electrons (N ≈10). This barrier is commonly referred to as the exponential wall because of the exponential component in (2.33) [29].

Because a multi-electrode wave function cannot be fully characterized by a single Slater determinant, the energy determined by HF calculations is always greater than the precise ground state energy. The Hartree-Fock limit is the highest precise energy available using HF methods [21].

The difference between $E_{HF}\ and\ E_{exact}$ is called correlation energy and can be expressed as[30]

$$E_{corr}^{HF} = E_{min} - E_{HF} \tag{2.34}$$

The mean-field approximation utilized in the HF method contributes the most to the correlation energy. That is one electron moves in the average field of the others, a method that ignores the fundamental connection between electron motions. To better grasp what this implies, consider electron repulsion at short distances, which is not addressed by a mean-field technique like the Hartree-Fock method [21].

Chapter 3

Density functional theory

3.1 A new base variable – the electron density

A general statement concerning the computation of observables has been presented in section 2.3 about the wave function ψ. This section is about a quantity that is computed in a similar manner. The electron density (for N electrons) as the fundamental variable of density functional theory is stated as [21,31]

$$\mathrm{n}(\vec{r}) = N \sum_{s1} \int d\vec{x}_2 \ldots \int d\vec{x}_N \, \psi^*(\vec{x}_1, \vec{x}_2, \ldots, \vec{x}_N) \, \psi(\vec{x}_1, \vec{x}_2, \ldots, \vec{x}_N) \tag{3.1}$$

It's worth noting that the notation in (3.1) takes into account a wave function with spin and spatial coordinates. In more detail, the integral in the equation represents the chance of finding a certain electron with any spin in the volume element $d\vec{r}_1$. Because electrons are indistinguishable, N times the integral equals the likelihood of finding any electron there. Other electrons with arbitrary spin and spatial coordinates are represented by the wave function $\psi(\vec{x}_1, \vec{x}_2, \ldots, \vec{x}_N)$ [21].

If the spin coordinates are not taken into account, the electron density can be described as a quantifiable observable that is simply reliant on spatial coordinates [31].

$$n(\vec{r}) = N \int d\vec{r}_2 \dots \int d\vec{r}_N \, \psi^*(\vec{r}_1, \vec{r}_2, \dots, \vec{r}_N)\psi(\vec{r}_1, \vec{r}_2, \dots, \vec{r}_N), \tag{3.2}$$

which can e.g. be determined by X-ray diffraction [21].

Before providing a method that uses electron density as a variable, make sure it has all of the relevant system information. That is to say, it must include information on the electron number N as well as the external potential, which is denoted by $\hat{V}$ [21].

Integrating the electron density across the geographical variables yields the total number of electrons [21].

$$N = \int d\vec{r}_N \, (\vec{r}). \tag{3.3}$$

What has to be demonstrated is that the electron density uniquely characterizes the external potential, up to a certain additive constant.

3.2 Thomas-Fermi theory

In quantum equations, the Thomas-Fermi theory was the first to use electron density as a variable rather than the wave function. The theory is based on interacting electrons traveling in an external potential field, and it offers a very basic explanation of electronic energy in terms of electron density distribution n(r): [32]

$$n(r) = \gamma(\mu - v_{eff}(r))^{\frac{3}{2}} \tag{3.4}$$

$$v_{eff}(r) = v(r) + \int \frac{n(r')}{|r-r'|} dr' \tag{3.5}$$

In equation (3.4) μ is the coordinate-independent chemical potential and r is a constant. The variations between external potential (the first term) and the electrostatic energy that is generated by the electron density distribution n(r) (the second term) calculate in equation (3.5). The number of electrons in a small enough distance element dr is homogeneous and can be expressed as n(r) dr. So the energy of the system can be calculated by:

$$E_{TF}[n(r)] = \int \frac{3}{10}(3\pi^2)^{\frac{2}{3}} n(r)^{\frac{5}{3}} dr + \int v(r)\, n(r) dr + \frac{1}{2}\int \frac{n(r)n(r')}{|r-r'|} dr dr', \tag{3.6}$$

Where the first term is the electronic kinetic energy calculated by integrating the kinetic energy density of a homogeneous electron gas.

The Thomas-Fermi theory made a significant breakthrough in that it provided a crude form of expressing the solution of the many-electron Schrodinger's equation in terms of electron density *n(r)* rather than wavefunction ψ, allowing us to characterize the electronic structure of the system simply by knowing the electron density *n(r)*. However, because Equation (3.4) is predicated on the formulation of a uniform electron gas distribution under an external potential, the theory has several flaws. First, the v_{eff} percent gradients were blatantly neglected. As a result, the theory is limited to systems with slowly fluctuating densities. Second, kinetic energy is described in a very rudimentary manner. Because kinetic energy accounts for a significant amount of a system's overall energy, a little inaccuracy of kinetic energy descriptions for each location might have severe consequences. As a result, it's only useful for characterizing energy's qualitative patterns. The electron-electron interaction is also too simplified. Because these interactions were considered conventionally, much of the quantum phenomena were overlooked. Chemical bonding is completely ignored by the hypothesis. Although the gradient, exchange, and correlation were added subsequently to improve the approach, it was still regarded as too crude for electoral structure computation applications [33,34].

3.3 Hohenberg-Kohn Theory

Uniqueness: The demonstration of "the ground state density *n(r)* of a bound system of interacting electrons in an external potential *v(r)* defines this potential uniquely" is the first major lemma of the Hohenberg-Kohn theory. The demonstration of this lemma was as simple as assuming an electron density n(r), which equates to two non-degenerate ground state potentials $v_1 r$ and $v_2 r$ with ground state wavefunction of Ψ_1 and Ψ_2, respectively. The ground state energies E_1 and E_2 were computed using two different potentials and wavefunction but the same electron density generated $E_1 + E_2 < E_1 + E_2$, defying the premise that two states are non-degenerate. As a result, the ground state electron density $n_o(r)$ may be used to calculate the ground state [31].

Variational Theory: The anticipated value of the Hamiltonian for a trial wavefunction must be bigger than or equal to the actual ground state energy, according to variational theory, which is particularly beneficial in many quantum methods. If the ground-state electron density $n_o(r)$ is known, the ground state energy may be solved using the uniqueness theorem. By layering on the Variational Theory, the ground state energy may be calculated by minimizing the energy

in terms of electron density n(r). The energy may be expressed as a sum of kinetic energy, electrostatic energy, and the energy of a noninteracting electron traveling under a potential difference:

$$E_{[n(r)]} = T_{[n(r)]} + U_{[n(r)]} + \int V(\vec{r})\, n(\vec{r}) d^3r, \tag{3.7}$$

Where the first two components are independent of the external potential *V(r)* and may be represented using an electron density universal functional *n(r)*:

$$T = \int \frac{3}{10} [3\pi^2 n(r)]^{\frac{2}{3}} n(r) dr \tag{3.8}$$

$$U = \frac{1}{2} \int \frac{n(r')}{|r-r'|} dr' dr \tag{3.9}$$

As a result, the Hohenberg-Kohn Theory gave us a way to calculate the energy in terms of electron density. However, the approach is inaccurate due to an insufficient representation of kinetic energy T [32].

3.4 Kohn-Sham Equations

The Kohn-Sham theorem states that if we can discover the real ground-state electron density, we can find the lowest energy of the system and consequently the ground state of the system, following the Hohenberg-Kohn theorem. The theorem also provides a method for determining the density of the ground state. The ground state energy, according to Kohn and Sham, may be represented as a function of the charge density:

$$E_{[n(r)]} = T_{[n(r)]} + \frac{1}{2} \int \frac{n(r) n(r')}{|r-r'|} + v_{xc[n(r)]} \tag{3.10}$$

where the kinetic energy is the first term, while the interaction between the electron and the external potential is the second term. Electron-electron electrostatic interaction and non-classical exchange-correlation energy are the third and fourth terms, respectively. The electron-electron interaction is described by the last two terms together. Hartree's self-consisting single-particle equations for approximating the electrical structure were an inspiration where every electron was regarded as moving in an effective single-particle potential, Kohn and Sham then reintroduced the single-particle wavefunctions: [35,36]

$$n(r) = \sum_{i=1}^{n} \psi_i^*(r) \psi_i\,(r). \tag{3.11}$$

The kinetic energy can be written in terms of wavefunctions by:

$$T[n(r)] = -\frac{\hbar^2}{2m}\sum_{i=1}^{n}\langle\psi_i|\nabla^2|\psi_i\rangle. \tag{3.12}$$

Equation

$$\int \psi_i^*(r)\,\psi_j\,(r)dr = \delta_{ij} \tag{3.13}$$

ensures that the wavefunctions are orthonormal. The solutions to Schrödinger's equation of non-interacting particles traveling in an effective potential $v_{eff}(r)$ are these wavefunctions:

$$-\frac{\hbar^2}{2m}\nabla^2\psi_i(r) + v_{eff}(r)\psi_i(r) = \varepsilon_i\psi_i(r), \tag{3.14}$$

where $$v_{eff}(r) = v_{ext}(r) + v_{xc}(r) + \frac{1}{2}\int\frac{n(r')}{|r-r'|}dr'. \tag{3.15}$$

The exchange-correlation potential is given by:

$$v_{xc}(r) = \frac{\delta E_{xc[n(r)]}}{\delta n(r)} \tag{3.16}$$

So the energy of the system can be written as:

$$E_n = \sum_{i=1}^{n}\varepsilon_i - \frac{1}{2}\int\frac{n(r')}{|r-r'|} + E_{xc[n(r)]} - \int\frac{\delta E_{xc[n(r)]}}{\delta n(r)}n(r)dr, \tag{3.17}$$

Where ε_is are the eigenvalues of the non-interacting single-particle equation which is supposed to be an appropriate term.

The focus shifted to the particular shape of the exchange-correlation functional at this point. In fact, the precision of this approximation factor is so crucial that the actual usage of the ground state DFT is totally dependent on it. If each term in the Kohn-Sham energy functional was known, we would be able to obtain the exact ground state density and total energy. Unfortunately, there is one unknown term, the exchange-correlation (XC) functional (E_{xc}). E_{xc} includes the non-classical aspects of the electron interaction along with the component of the kinetic energy of the real system different from the fictitious non-interacting system. Since E_{xc} is not known exactly, it is necessary to approximate it.

3.5 Solving the Kohn-Sham equation

Self-consistent computations are used to solve the KS equation [37–39]. The potential in the KS equation depends on electron density. The electron density, on the other hand, is calculated using wavefunctions, which are dependent on the potential. At the start of the calculation, an estimate of electron density is made.

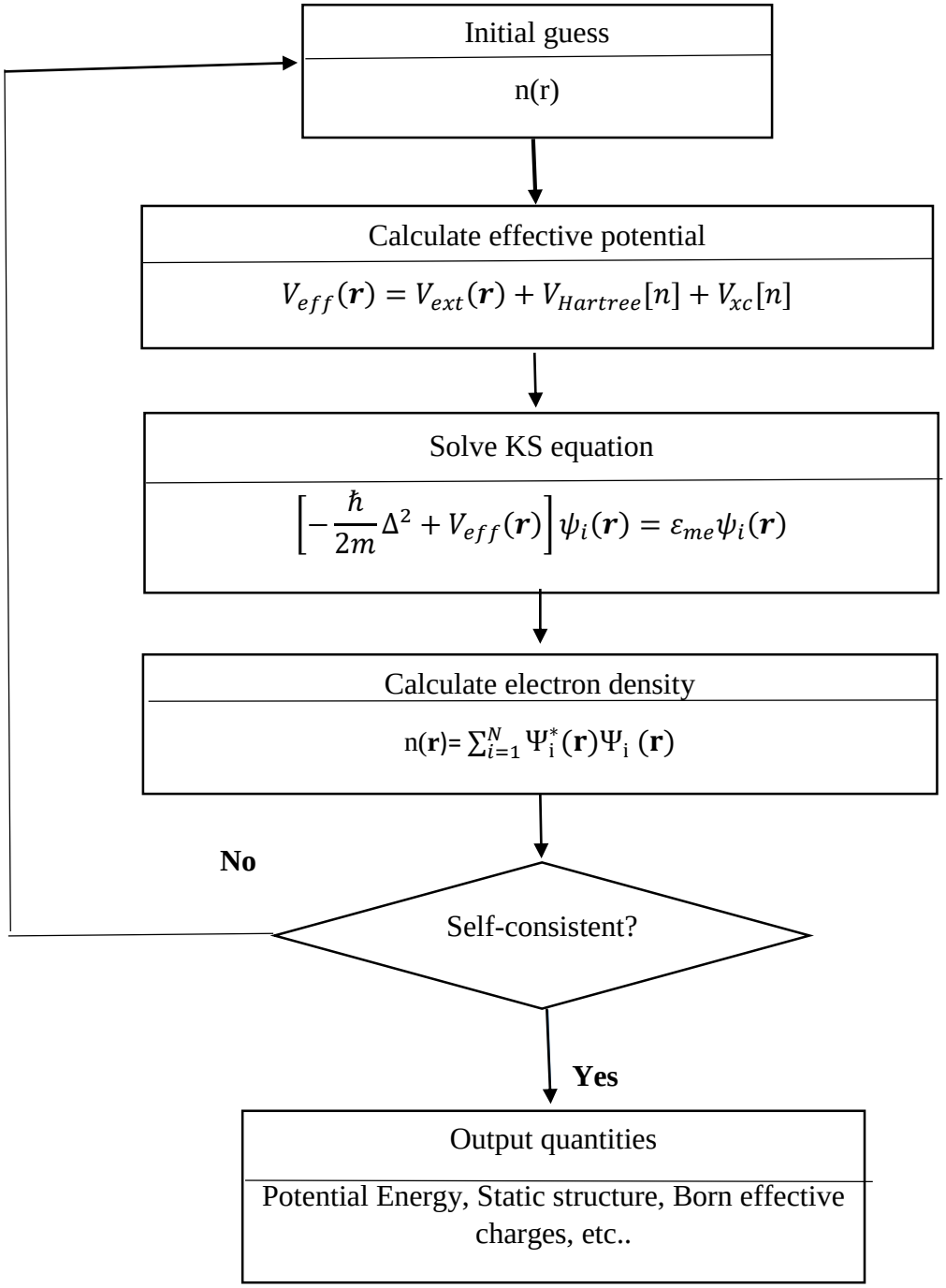

Figure 3.1: Self-consistent calculations and relaxation for solving the KS equation.

The KS equation is then solved for each k-point. The diagonalization of the Hamiltonian matrix yields eigenvalues and eigenfunctions. Those values and functions are used to determine total energy and fresh charge density. If the density and total energy do not converge, the effective potential is recalculated using the new density, which is usually a combination of the old and new density. As a result, this method is a self-contained calculating method. In addition, the forces on atoms must be converged to a sufficiently minimal value for ion and lattice relaxation.

3.6 Exchange-correlation potential

Because the exact shape of the exchange-correlation potential is unknown today, it is the most difficult portion of the KS equation to solve. Therefore, there are different approximations to it, such as the local density approximation (LDA), generalized gradient approximation (GGA), and hybrid functional approach, such as HSE06 [39].

3.6.1 Local density approximation (LDA)

The LDA is a simple approach to estimate the exchange-correlation portion and is a first rough approximation. It is based on the free homogeneous electron gas hypothesis, which has a constant electron density

$$\rho(\boldsymbol{r}) = \rho = \frac{N}{V} \tag{3.18}$$

Here, N is a number of electrons in the solid with volume V. The one possible expression of LDA exchange-correlation energies are given as [40–42]

$$\varepsilon_{xc}^{gas}(\rho) = -\frac{3}{4} \cdot \frac{3^{\frac{1}{3}}}{\pi} \cdot \rho^{\frac{1}{3}} + \begin{cases} Alnr_s + B + Cr_s lnr_s + Dr_s & if\ r_s \leq 1 \\ \gamma\ /(1 + \beta_1\sqrt{r_s} + \beta_{2r_s} & if\ r_s > 1 \end{cases} \tag{3.19}$$

Here, $r_s = 3/(4\pi\rho)^{\frac{1}{3}}$; A, B, C, D, γ, β_1 and β_2 are parameters [40–42]. According to the LDA, the exchange-correlation energy for an electron in a very small tiny volume in a many-particle system is equivalent to the exchange-correlation energy for an electron in a free electron gas with the same density in the volume ($\varepsilon_{\mathrm{xc}}^{\mathrm{gas}}\big(\rho(\mathbf{r})\big) = \varepsilon_{\mathrm{xc}}^{\mathrm{gas}}(\mathbf{r})$). The explicit exchange-correlation energy is given as

$$E_{xc}^{LDA}[\rho] = \int \rho(\boldsymbol{r})\, \varepsilon_{xc}^{gas}(\boldsymbol{r}) d\boldsymbol{r} \tag{3.20}$$

The corresponding exchange-correlation potential is given by

$$V_{xc}^{gas}(\boldsymbol{r}) = \frac{\delta E_{xc}^{LDA}[\rho]}{\delta \rho} \tag{3.21}$$

The generalized gradient approximation $\mathrm{E_{xc}^{LDA}}[\rho]$ is the second family of approximations, in which the density gradient is also taken into consideration to calculate the exchange-correlation energy.

The total energy of a solid is reasonably adequately described by both LDA and GGA.

3.6.2 Hybrid functional approach (HSE06)

Another approximation approach $\mathrm{E_{xc}}[\rho]$is to calculate the exchange energy precisely within the Hartree-Fock approximation, then apply an estimate for the correlation energy. The band gap energies produced by this exchange-energy approach are often excessively big. It is occasionally preferable to use a combination of the exchange-energy approach and the LDA or GGA. This is so called hybrid functional approach, where the exchange energy is mixed in order to empirically obtain better energies and band gap energies. In HSE06 method, the following equation is defined as

$$E_{xc}^{HSE}[\rho] = \alpha E_{xc}^{SR}(\mu) + (1-\alpha) E_{x}^{PBE,SR}(\mu) + E_{x}^{PBE,LR}(\mu) + E_{c}^{PBE} \tag{3.22}$$

Here, the short range (SR) part of the exact exchange $\mathrm{E_x^{SR}}$ is mixed with a short range part of the GGA exchange $E_x^{PBE,SR}$ by Perdew, Burke and Erzerhof (PBE) [39]. The correlation part of the electron-electron interaction is obtained from the PBE approximation $\mathrm{E_c^{PBE}}$.

Many alternative exchange-correlation potentials exist today. It is still under construction. The KS equation has the advantage of being simple to implement additional potentials. However, because of the ease of implementation, various potentials exist, which might be viewed as inconsistent [39].

3.6.3 The Generalized-Gradient Approximation (GGA)

It was understood very early that only the local uniform density at each given point is not a reasonable approximation for the rapidly changing electron densities of many materials, and that the gradient of the density ($\nabla n(r)$) needs to be included. A first attempt was the so-called gradient-expansion approximations (GEA). The idea behind GEA is to regard LDA as the term in a power series expansion of E_{xc} in the density's spatial variation (described by the derivatives of n(**r**)). The second-order GEA thus uses LDA plus the term of next lowest order in density variation, giving a functional of the form

$$E_{xc}^{GEA}[n] = E_{xc}^{LDA}[n] + \int A_{xc}\big(n(\boldsymbol{r})\big)s^2 + \int B_{xc}\big(n(\boldsymbol{r})\big)q + \cdots \tag{3.23}$$

Where $A_{xc}\big(n(\boldsymbol{r})\big)$ and $B_{xc}\big(n(\boldsymbol{r})\big)$ are dimensionless functions of $n(\boldsymbol{r})$, and s and q defines the appropriate measure of the density gradient both of which have been expressed on scale-invariant form; the dimensionless gradient

$$s = \frac{|\nabla n|}{2k_F n} = \frac{|\nabla n(\boldsymbol{r})|}{2(3\pi^2)^{\frac{1}{3}} n^{\frac{4}{3}}(\boldsymbol{r})} = \frac{3}{2}\frac{4}{9\pi}^{\frac{1}{3}} |\nabla r_s| \tag{3.24}$$

and the dimensionless Laplacian

$$q = \frac{\nabla^2}{2{k_F}^2 n} = \frac{\nabla^2 n(\boldsymbol{r})}{4(3\pi^2)^{\frac{2}{3}} n^{\frac{5}{3}}(\boldsymbol{r})} \tag{3.25}$$

Because there is no special direction in the uniform electron gas, there can be no term linear in ∇n. Moreover, terms linear in $\nabla^2 n$ can be recast as s^2 terms via integration by parts, since:

$$\int d\boldsymbol{r}\, f(n)\nabla^2 n = -\int d\boldsymbol{r} \left(\frac{\partial f}{\partial n}\right) |\nabla_n|^2 \tag{3.26}$$

In application to real systems, the GEA has generally been disappointing, indeed often worsened the results of the LDA. The failure of the GEA leads to the development of generalized-gradient approximation (GGA). The XC functional is written as a function of the local density and the local gradient of the density, usually, as an "enhancement factor" F_{xc} multiplying the homogeneous electron:

$$E_{xc}^{GEA}[n] = \int \in_{xc} \big(n(\boldsymbol{r})\big) F_{xc}\big(n(\boldsymbol{r}), \nabla n(\boldsymbol{r})\big) d\boldsymbol{r} \tag{3.27}$$

The enhancement factor is written in terms of r_s and the dimensionless density gradient s:

$$F_{xc}(n(\boldsymbol{r}), |\nabla n(\boldsymbol{r})| \rightarrow F_{xc}(r_s, s)$$

Gradient-corrected functionals are the simplest extensions of LDA to inhomogeneous systems one can think of. GGA found widespread acceptance due to its improved performance. GGA functionals are known to satisfy some known conditions that the exact functional should satisfy as well [16]. They yield much better atomic energies and binding energies than LDA, at a modest additional computational cost [43,44].

Chapter 4

Results and Discussion

4.1 Geometric structure and volume optimization

Basic input parameters such as lattice constants and Wyckoff positions were mostly obtained from prior work for the calculations of structural, electrical, optical, and elastic characteristics of cubic $NaMCl_3$ (M =In, Al), with space group of Pm-3m (221) [6].

Table 4.1 Optimized lattice parameters and Wyckoff positions for cubic $NaMCl_3$ (M =In, Al).

Perovskite Compounds	Optimized Lattice Parameters (Å)	Wyckoff Positions			
		Atom	x	y	z
$NaInCl_3$	5.4030	Na	0	0	0
		In	0.5	0.5	0.5
		Cl	0.5	0.5	0
$NaAlCl_3$	5.0420	Na	0	0	0
		Al	0.5	0.5	0.5
		Cl	0.5	0.5	0

First, energy v/s volume optimization calculations for all of the examined compounds were done to obtain the appropriate precision for all of the studied characteristics. Table 4.1 summarizes the obtained optimal lattice parameters, as well as the theoretical values and Wyckoff locations. $NaMCl_3$ (M =In, Al) compounds have cubic crystal structures in which Na atoms are present at corner positions, and the X atom is presented at the body center position, while Cl atoms are located at the middle of the edges. The crystal structure of both compounds $NaInCl_3$ and $NaAlCl_3$ are same. So we expressed the structure in one common figure. Crystalline structures are drawn by using the XCrySDen software [45] and the structure is presented in Figure 4.1. For obtaining the values of the parameters for example lattice constants at the lowest energy state, we have optimized structures using the PBE-GGA approximation. Minimum values for the radius of muffin-tin (R_{MT}) for Na, In, Cl, was taken 2.3, 2.3, 2.3 a.u respectively for $NaInCl_3$ material. In case of NaAlCl3 material the R_{MT} values for Na, Al, Cl was taken 2.50, 2.32, 2.32 a.u respectively. The angle of cubic perovskite were taken as 90° for both materials.

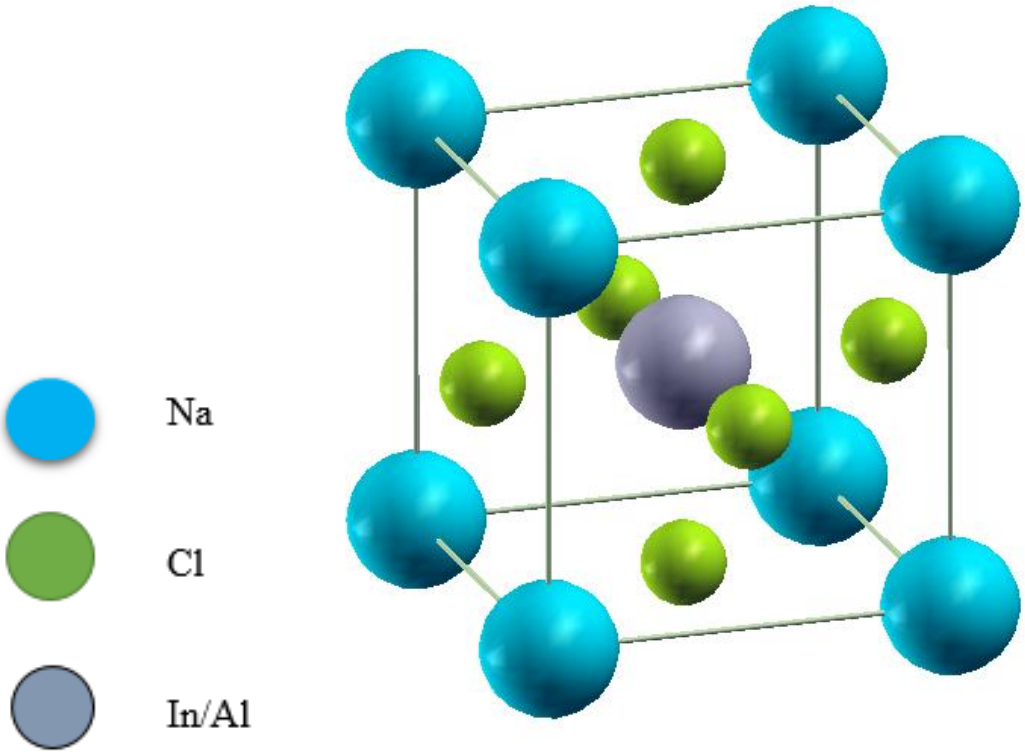

Figure 4.1: Crystal Structure of cubic $NaMCl_3$ (M =In, Al)

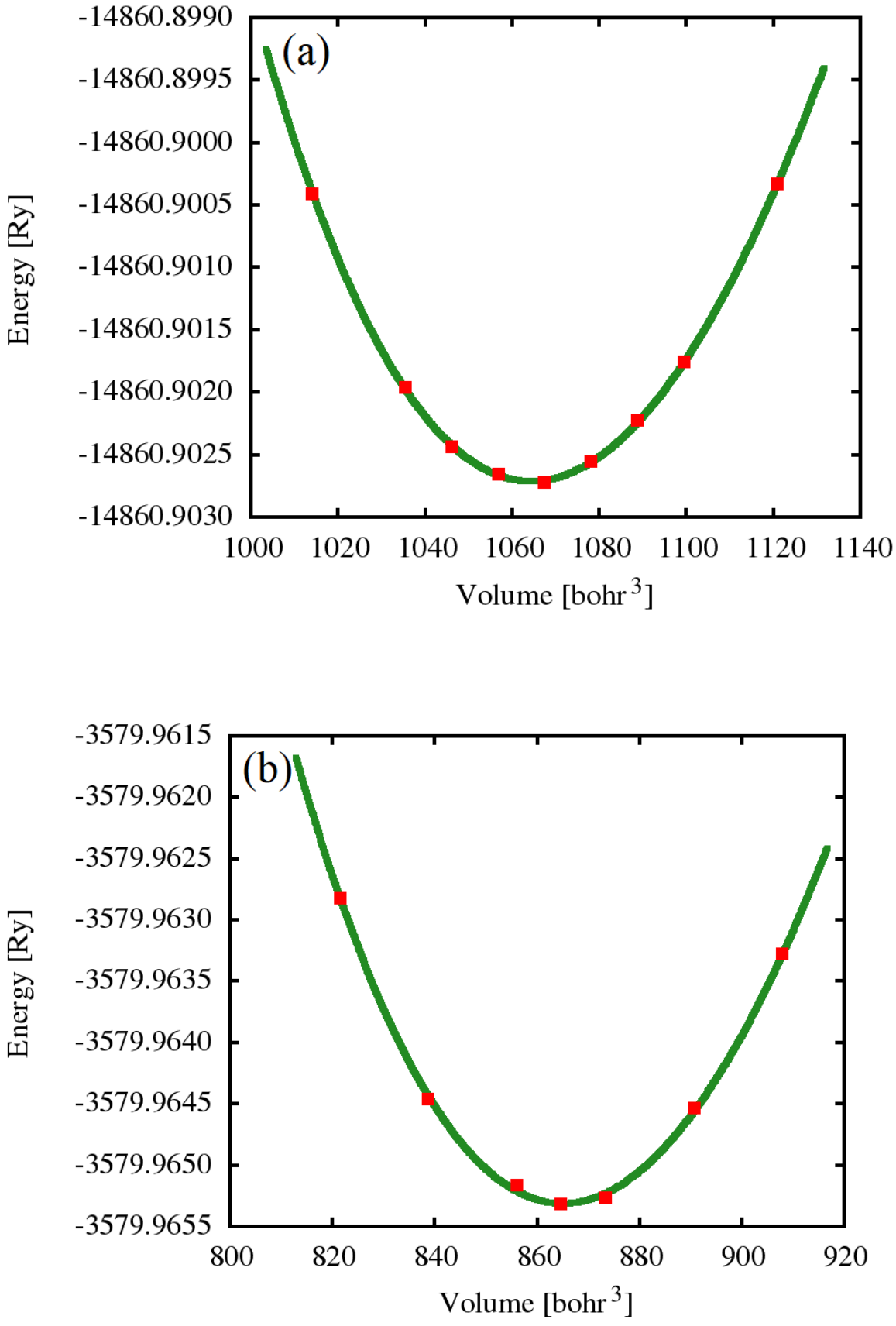

Figure 4.2: Energy v/s volume optimization curves for (a) $NaInCl_3$ and (b) $NaAlCl_3$.

For volume optimization, we took the RK_{MAX} value as 8.5, where $RK_{MAX} = R_{MT} \times K_{MAX}$. Here R_{MT} represents radius of muffin-tin (MT) radius of the non-overlapping atomic sphere which is the smallest size neutral atoms and K_{MAX} represents the largest value of the reciprocal lattice vector [6]. Other parameters considered in present calculations include variables such as 1000 k-points, $G_{MAX} = 12(a.u.)^{-1}$ $l_{max} = 10.0$. To confirm the accuracy of calculations, cutoff values for energy, forces, and core and valence state's separation were kept as 0.0001 Ry, 1 mRy/a.u. and -6.0 Ry, respectively.

4.2 Self Consistent Field (SCF) calculation

After volume optimization, we used the optimized lattice parameter from the outputeous file for regenerating the structures of $NaMCl_3$ (M =In, Al). Before SCF calculation we initialized with appropriate parameters and do the non-magnetic calculation with PBE potential. The parameters we used for the initialization of SCF calculation are listed in Table 4.2.

Table 4.2 Parameter used in SCF (PBE) calculation of $NaMCl_3$ (M =In, Al).

Perovskite Compounds	Optimized lattice parameter(Å)	RMT	
$NaInCl_3$	5.4030	Na	2.3
		In	2.3
		Cl	2.3
$NaAlCl_3$	5.0420	Na	2.5
		Al	2.32
		Cl	2.32

Self-consistent field (SCF) methods include both Hartree-Fock (HF) theory and Kohn-Sham (KS) density functional theory (DFT). Self-consistent field theories only depend on the electronic density matrices and are the simplest level of quantum chemical models. The RK_{MAX} values we used in the calculation for both $NaMCl_3$ (M =In, Al) materials were taken 8.5. The energy convergence criteria were 0.0001 Ry for $NaInCl_3$ and 0.0001 Ry for $NaAlCl_3$. We also took the k-points value as 1000 and l-max value as 10 for both materials.

Once the SCF cycle has converged one can calculate various properties like band structure, Density of States (DOS), Optical properties, Elastic constants, etc. From the SCF calculation, we found band gap, total energy, Fermi energy. These values are listed in Table 4.3.

Table 4.3 Calculated band gap (eV), Total energy (eV) and Fermi Energy (eV) of $NaMCl_3$ (M =In, Al) using PBE-GGA potential.

Compounds	Band gap (eV)	Fermi energy (eV)	Total energy (eV)
$NaInCl_3$	0	0.1176390100	-202192.95517
$NaAlCl_3$	0	0.2348555241	-48707.925785

4.3 Energy band structure

The quantum-mechanical behavior of electrons in solids is described by a theory or band structure. Electrons in solitary atoms have only a few discrete energies, which may be shown as a sequence of distinct lines on an energy-level diagram. We used the most accurate exchange and correlation functions to compute structural parameters of perovskite $NaMCl_3$ (M =In, Al) materials, as mentioned in the preceding section.

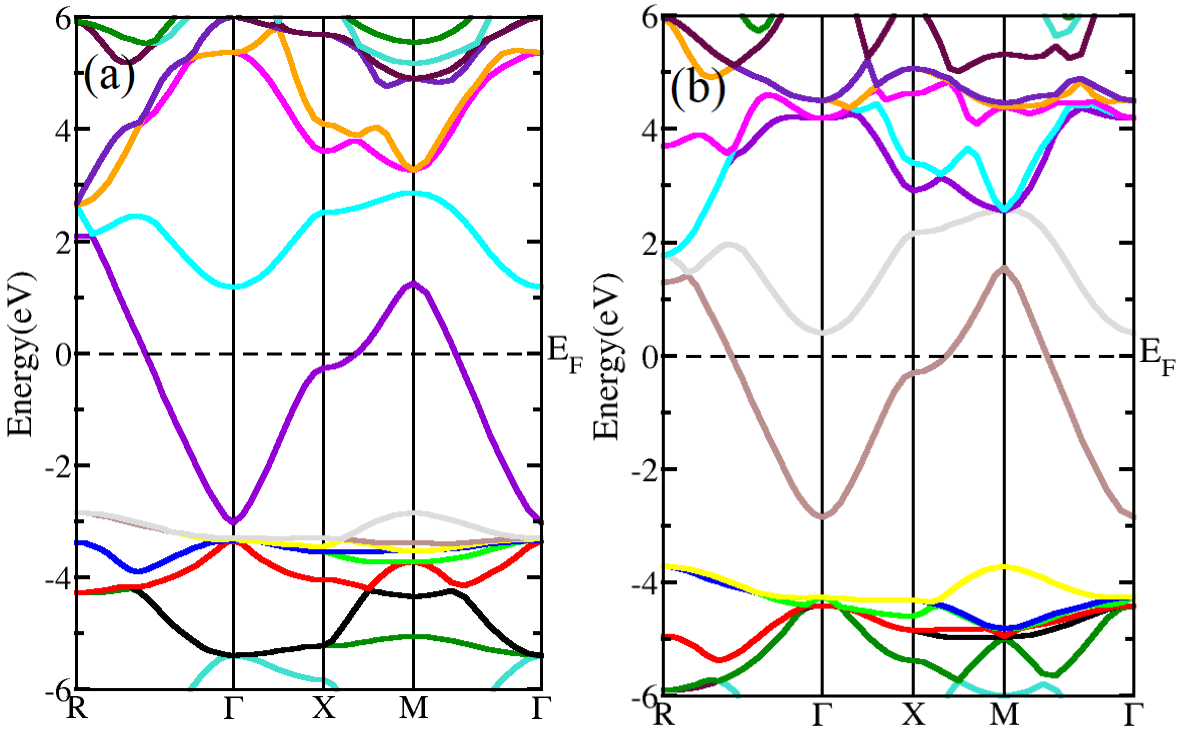

Figure 4.3: Estimated Band structure of (a) $NaInCl_3$ and (b) $NaAlCl_3$

Calculations are also carried out to identify the energy band gap, electronic response, and energy band structures of all the compounds evaluated. Band structure of the compounds attained within the framework of PBE-GGA described in Figure 4.3. From the Figure 4.3, we see that both the materials have no band gap at the Fermi level. The conduction band crosses the Fermi level and enters into the valence band. So the band gap is zero here. We know that metal has no band gap at the Fermi level. Generally, we found band gaps in semiconductors and insulators. So from figure 4.3, we can say both $NaInCl_3$ and $NaAlCl_3$ are metals. Good metal conductors have a zero band gap, which means that these materials can be used to produce electrical wires and other electrical devices. Their valence and conduction bands overlap at the Γ points.

4.4 Density of States (DOS)

The density of states (DOS) is the number of distinct states that electrons can occupy at a given energy level or the number of electron states per unit volume per unit energy. This function is responsible for bulk properties of conductive substances like specific heat, paramagnetic susceptibility, and other transport phenomena. DOS calculations can be used to figure out the general distribution of states as a function of energy and the spacing between energy bands in semiconductors [46].

For detailed investigations of the formation of energy bands, one needs to compute the Density of States (DOS). The calculated DOS for compounds $NaMCl_3$ (M =In, Al) are shown in Figure 4.4. From the above figure 4.4, we see the total density of states and atoms individual contributions of $NaMCl_3$ (M =In, Al). In fig 4.4 the conduction band overlaps the Fermi level and enters into the valence band region. DOS contribution in the valence band region is higher than the conduction band. We get the higher peak of DOS in the valence band region. We plot DOS between -8 eV to 6 eV energy range. From the figure 4.4 (a) we can see that in case of $NaInCl_3$ the Cl atom contribution is higher than Na and In atom, but in figure 4.4 (b) we can see that Na atom contribution is higher than Al and Cl atom.

In $NaMCl_3$ (M =In, Al) systems, the Cl atom contribution in the DOS is higher than the other atoms. The Na atom contribution is very low in the valence band than the conduction band. From the Density of States plot, we can say that it is a good metal conductor as these materials have no energy gap at the Fermi level.

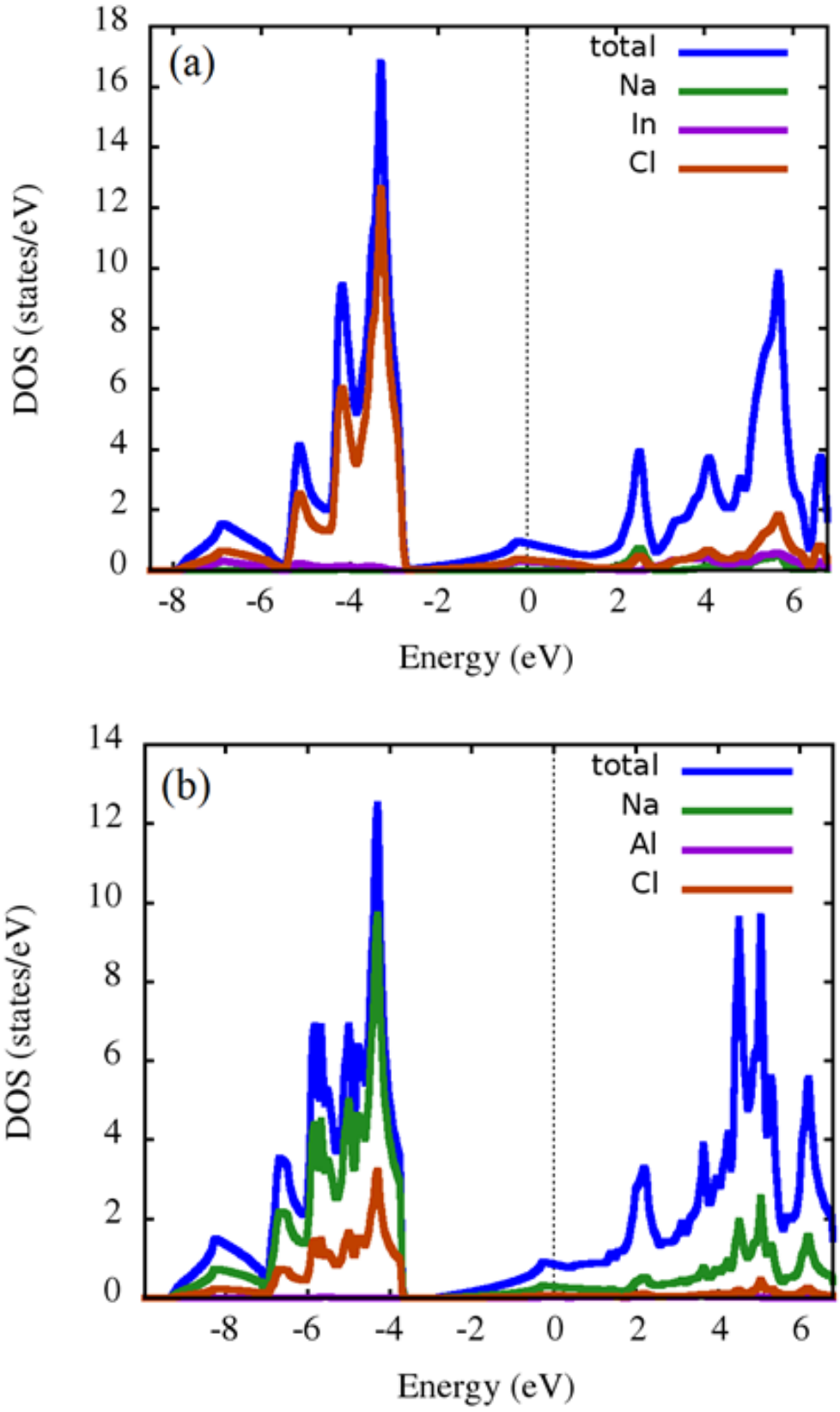

Figure 4.4: Density of States (DOS) of (a) $NaInCl_3$ and (b) $NaAlCl_3$

4.5 Optical Properties

A material's optical characteristics determine how it interacts with light. For optical properties calculation, we used k-points as 10000 for both materials. We found the plasma frequency as 2.984 for $NaInCl_3$ and 3.166 for $NaAlCl_3$. In this section, we discuss the optical properties of $NaMCl_3$ (M =In, Al) such as absorption coefficient, optical conductivity, optical reflectivity, refractive index, dielectric tensor, and electron energy loss.

4.5.1 The Absorption Coefficient

The absorption coefficient specifies how far light of a specific wavelength can reach into a substance before being absorbed. Light is only poorly absorbed in a material with a low absorption coefficient, thus it appears transparent to that wavelength if the substance is thin enough. The absorption coefficient is determined by the substance as well as the wavelength of the absorbed light. In metal perovskite materials $NaMCl_3$ (M =In, Al) the absorption coefficient increases with the increase of energy. Generally, metal conductors have a high absorption coefficient. Because light with energy below the band gap does not have enough energy to drive an electron from the valence band into the conduction band, semiconductor materials show a sharp edge in their absorption coefficient. As a result, there is no absorption of this light. The absorption coefficient is not constant for photons with energies above the band gap, although it is still substantially dependent on wavelength. The likelihood of absorbing a photon is proportional to the probability of a photon and an electron interacting in such a way that they migrate from one energy band to the next. Not only electrons with energies close to the band gap can interact with the photon as the photon's energy increases. As a result, more electrons may interact with the photon, causing it to be absorbed [24]. The absorption coefficient, α is related to the extinction coefficient, k by the following formula

$$\alpha = \frac{4\pi k}{\lambda}$$

This is the absorption coefficient equation. Where λ is the wavelength.

In figure 4.5 we can see the absorption coefficient of $NaMCl_3$ (M =In, Al) compounds. The range of photon energies for visible light is 1.63 eV to 3.26 eV. For both $NaMCl_3$ (M =In, Al) compounds the absorption coefficient is very weak in the visible light region. So we can say that these materials cannot absorb visible light.

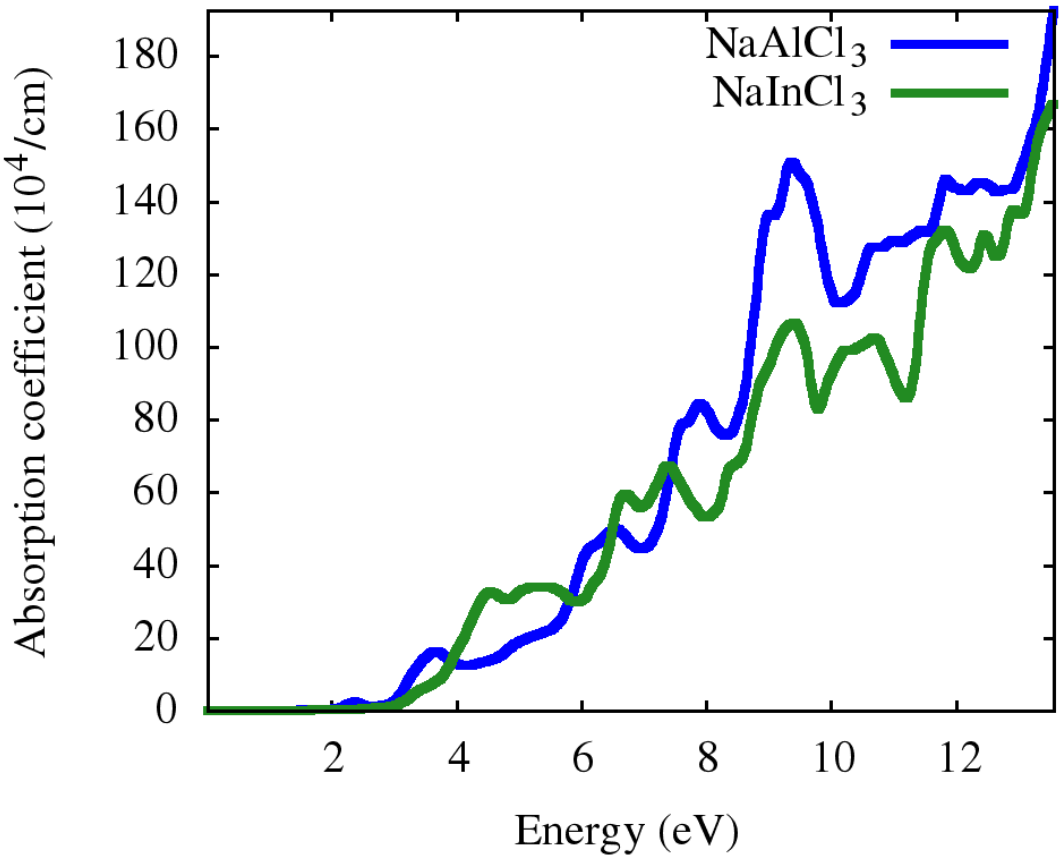

Figure 4.5: Optical absorption coefficient for $NaAlCl_3$ and $NaInCl_3$

So we can say that these materials cannot absorb visible light. But after the visible light region, the absorptivity starts to increase. So both $NaMCl_3$ (M =In, Al) absorbs mainly UV light. As the energy increases the absorptivity also increases in this region. From the figure, we can see that $NaAlCl_3$ gives a higher absorption coefficient than $NaInCl_3$. So we can say that, $NaAlCl_3$ absorbs more light. For metals, the absorptivity increases with the energy. Optical absorption provides essential information on the electronic properties of metals.

4.5.2 Optical Conductivity

Optical conductivity σ (ω) determines the ability of a medium to initiate a phenomenon of conduction as the electromagnetic radiations try to propagate through it. Calculations of optical properties of $NaMCl_3$ (M = In, Al) perovskite compounds, enable us to precisely explain their probable utilization in various optoelectronic applications. Fig-4.6 represents the optical conductivity at different energies of perovskites $NaMCl_3$ (M =In, Al) compounds. As electronic conduction is a matter of putting electrons in the conduction band, one other way to

achieve this goal is to give an electron bound to the atoms enough energy to break the bond and set it free to move.

From figure 4.6, it is clear that the optical conductivity increases as energy increases. The energy between 1.63 eV to 3.26 eV, the conductivity starts to decrease and becomes almost zero at 2eV energy, but after the visible range region conductivity increases. At zero energy position, we get the highest optical conductivity. Between 8 eV to 10 eV energy, we get the highest optical conductivity for both materials. From figure 4.6, we can say that $NaAlCl_3$ material is a better conductor than $NaInCl_3$ material.

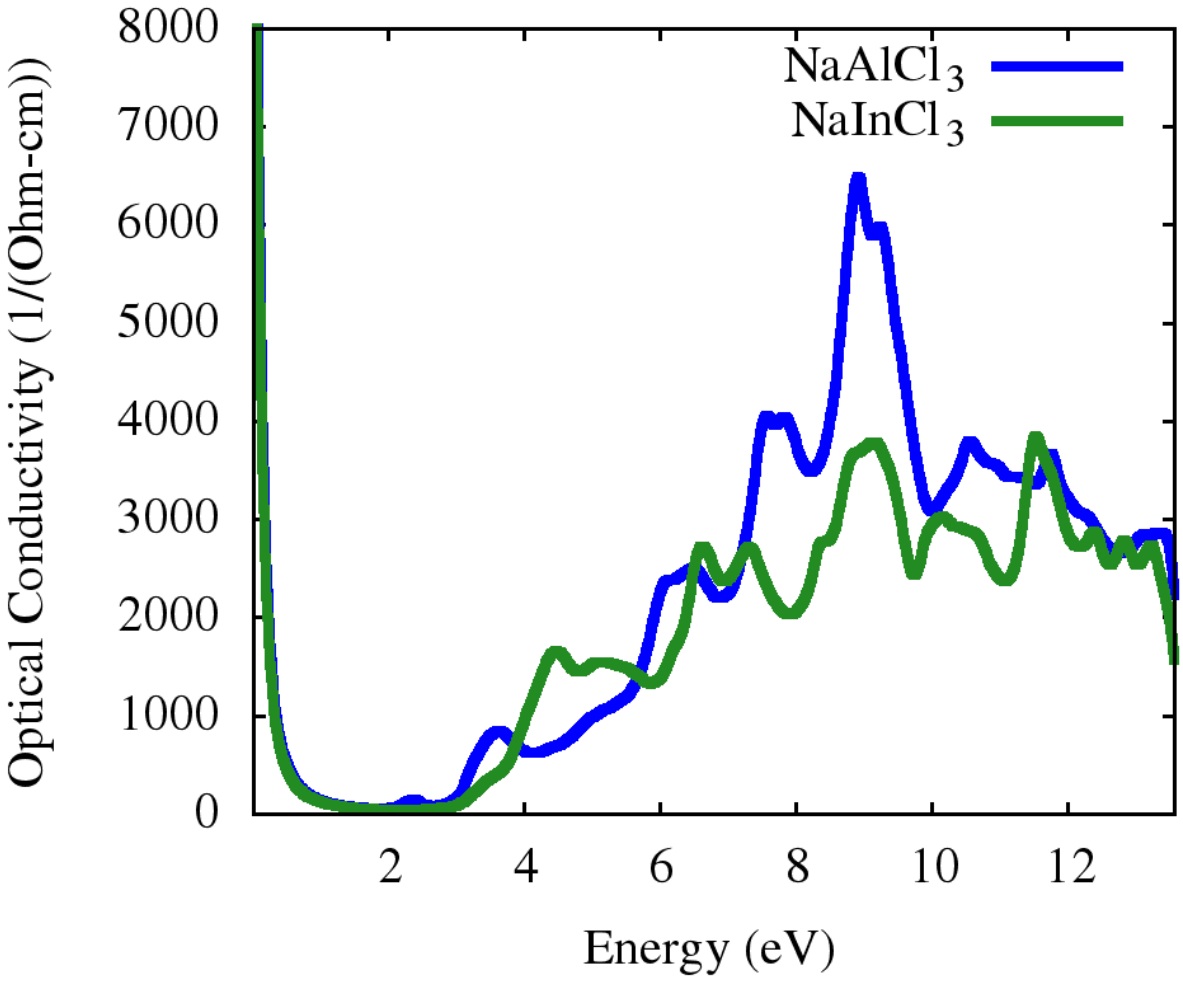

Figure 4.6: Optical Conductivity for $NaInCl_3$ and $NaAlCl_3$

4.5.3 Refractive index

The ratio of the speed of light in a vacuum to the speed of light in the second medium of larger density is used to compute the refractive index (also known as the Index of Refraction). The letter 'n' is the most popular symbol for the refractive index variable. The greater the deflection (or refraction) of a light beam entering or exiting a material, the higher its refractive index. We know that the refractive index means how fast light travels through the materials. The frequency of light traveling through a medium influences its refractive index (to some extent), with the highest frequencies having the greatest values of n. Figure 4.7 gives the relationship between the refractive index and the photon energy. From figure 4.7, we can see that both $NaInCl_3$ and $NaAlCl_3$ give the almost same result. The refractivity is maximum at 0 eV energy and minimum between 0.5 eV to 1.8 eV energy. After 12 eV energy the refractive index starts to decrease.

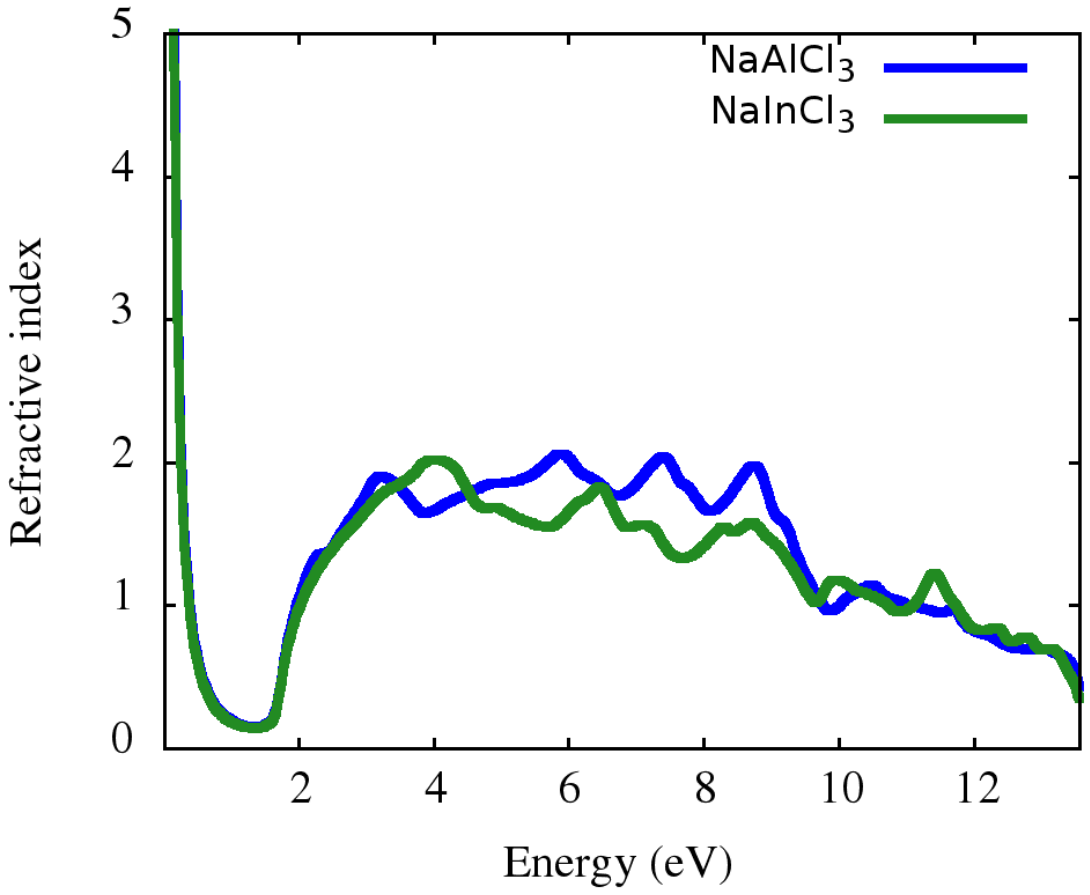

Figure 4.7: Refractive Index for $NaInCl_3$ and $NaAlCl_3$

4.5.4 Optical Reflectivity

This is a measure of a surface's capacity to reflect radiation, equivalent to the reflectance of a sufficiently thick layer of material for the reflectance to be independent of thickness. The reflectance and reflectivity spectra of each substance determine its potential as a perfect absorber. Furthermore, the total absorption (A), refraction (T), and reflectance (R) should equal 1 for improved optical resonance [6]. The reflectivity of light from a surface depends upon the angle of incidence and the plane of polarization of the light. The normal incidence reflectivity is dependent upon the indices of refraction of the two media. From figure 4.8, we see that at zero energy position the reflectivity is highest but after 0 eV position reflectivity starts to decrease and becomes zero at the 2 eV position. After, 2 eV positions the reflectivity again starts to increase. As the energy increases the reflectivity also increases after 2 eV energy. So from this property, we can say that $NaInCl_3$ and $NaAlCl_3$ are the good metallic reflector. Figure 4.8 is representing the optical reflectivity of $NaMCl_3$ (M =In, Al) compounds.

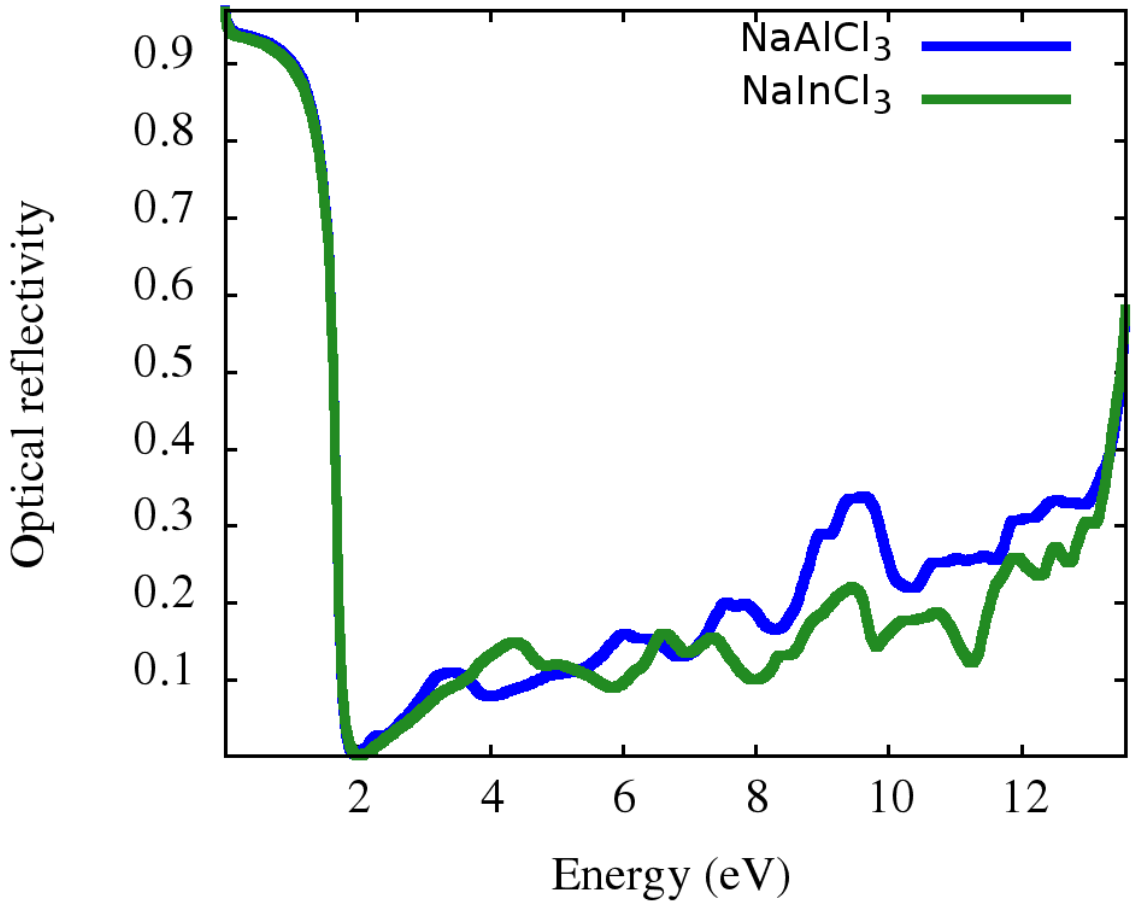

Figure 4.8: Optical reflectivity for $NaInCl_3$ and $NaAlCl_3$

4.5.5 Dielectric Function

The Dielectric Constant is a measurement of a substance's capacity to store electrical energy in an electric field. The dielectric constant is a complex quantity that may be represented as

$\varepsilon = \varepsilon_1 + i\varepsilon_2$, where ε_1 and ε_2 are the real and imaginary components of the dielectric constant, respectively. The optical response of the material to an electromagnetic field is described by the dielectric function [47]. Both the real and imaginary dielectric tensor for $NaInCl_3$ and $NaAlCl_3$ obtained from PBE-GGA potential. Both $NaMCl_3$ (M = In, Al) compounds give the almost same graph. From figure 4.9, we can say that $NaMCl_3$ (M = In, Al) compounds have negative real dielectric tensors before 2 eV energy. So, we cannot use these compounds to store electrical energy. After 2 eV energy, the real dielectric tensors starts to increase and we get positive value of real dielectric tensor. Again the real dielectric tensor starts to decrease after about 9 eV energy.

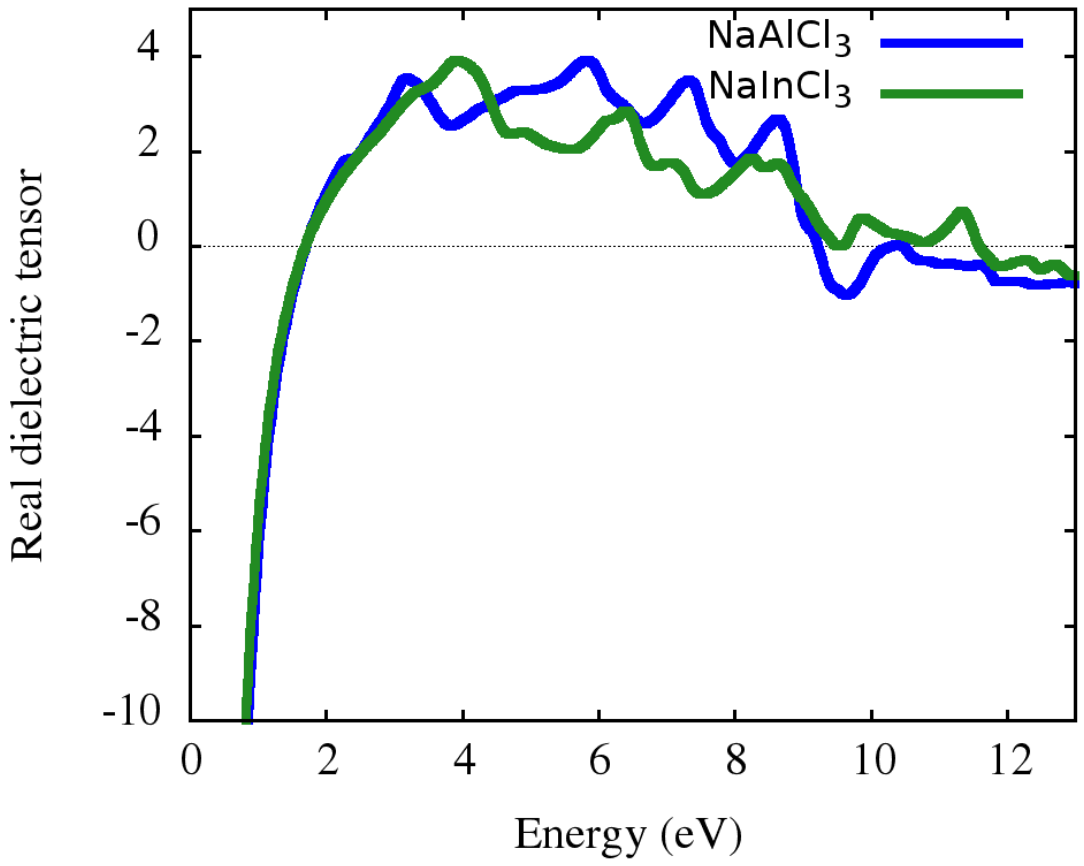

Figure 4.9: Real dielectric tensor for $NaInCl_3$ and $NaAlCl_3$

From fig 4.10, we can see that the imaginary dielectric tensor decreases suddenly between 0 to 3 eV energy. After about 3 eV energy, the imaginary dielectric tensor starts to increase and between 8 eV to 10 eV we can see a sharp peak.

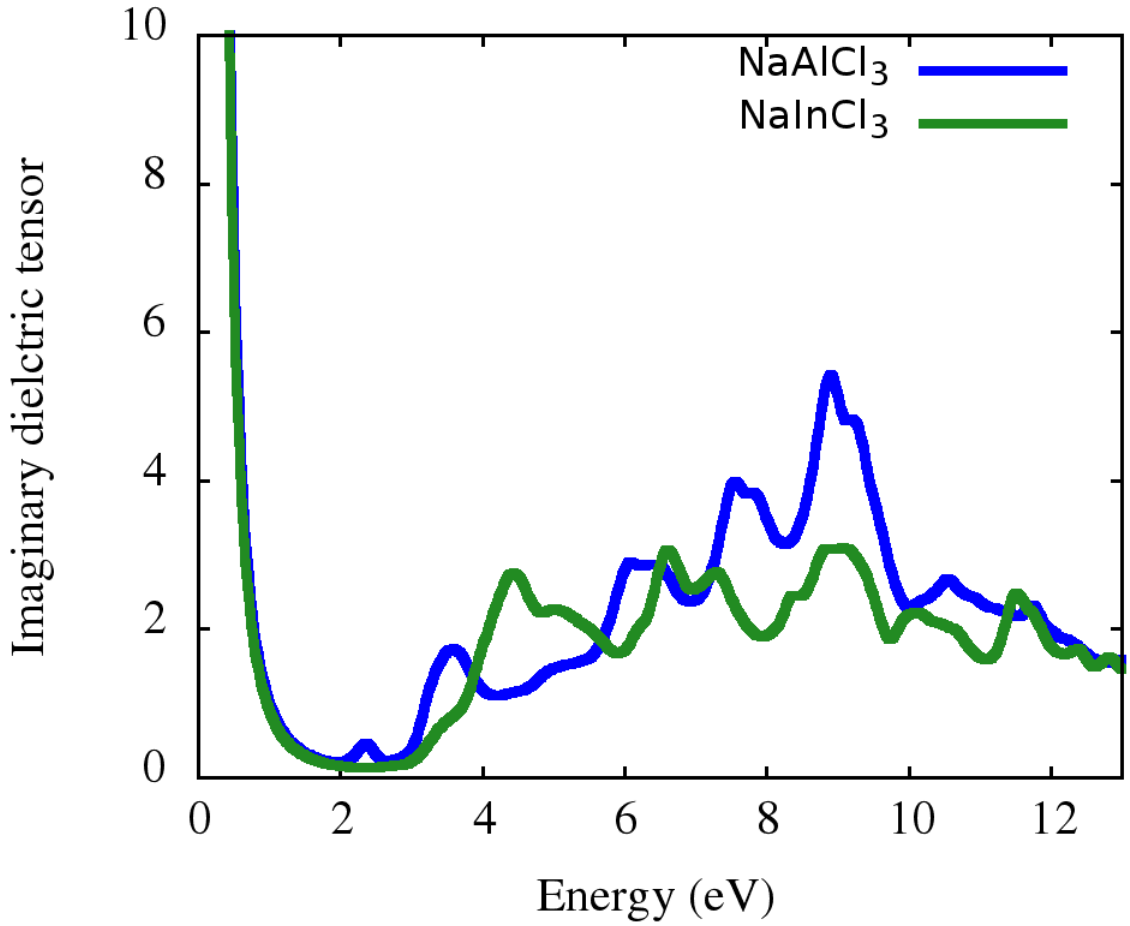

Figure 4.10: Imaginary dielectric tensor for $NaInCl_3$ and $NaAlCl_3$

4.5.6 Electron Energy Loss

The Electron Energy Loss (EEL) represents the probability that an incident electron loses energy and transfer a momentum per unit path length traveled in a solid. Electron energy spectroscopy is the utilize of the energy distribution of electrons that pass through a thin sample to analyze the content of the sample and produce images with unique contrast effects. Because the EEL is directly connected to the dielectric function, it may be used to determine a variety of dielectric characteristics of materials. Unfortunately, because the EEL is difficult to detect

experimentally, experimental data is not always accessible. Optical reflection and transmission measurements are commonly used to determine the EEL for zero momentum transfer. The energy loss function is directly related to the dielectric function, and hence many dielectric properties of materials can be extracted from the determination of the EEL. Unfortunately, experimental data for the EEL is not always available because it is difficult to determine experimentally. The EEL for zero momentum transfer is usually obtained from optical reflection and transmission measurement.

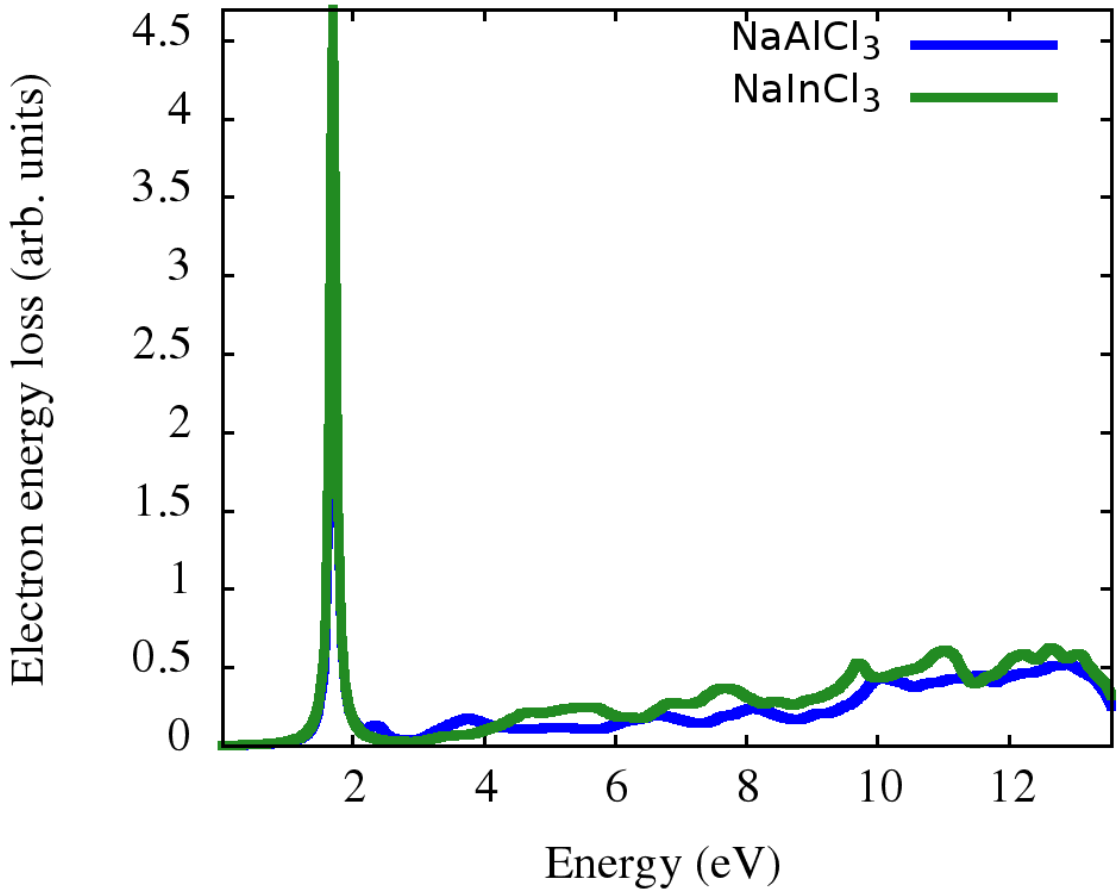

Figure 4.11: Electron energy loss for $NaInCl_3$ and $NaAlCl_3$

The energy loss function in all directions starts from zero (0) at 0 eV. From figure 4.10, we can see that the graph is almost the same for both materials. Between 1 eV to 2 eV, we have the highest energy loss of about 5. Almost 90% photon energy is needed to be absorbed by the electron for going to the next stable state.

4.6 Elastic Properties

The mechanical characteristics of $NaMCl_3$ (M = In, Al) are investigated using elastic constant calculations. The nature of bonding forces and mechanical stabilities is influenced by elastic constants. From the strain as a function of volume, the elastic constants C_{11}, C_{12}, and C_{44} were determined. The IRelast package, as implemented in WIEN2k, is used to examine elastic constants in this report. The following are the born stability conditions for cubic crystals [48–51]:

$$(C_{11} - C_{12}) > 0, C_{11} > 0, C_{44} > 0, (C_{11} + 2C_{12}) > 0$$

The estimated elastic constants satisfy the Born stability criterion, and these elastic constants are listed in Table 4. C_{11} represent resistance in x-direction under linear compression [52]. Similarly, C_{44} indicates the resistance to shear deformation under applied shear stress. In general, we state that C_{44} is concerned with the hardness of the material [53]. For both examined compounds, the value of C_{12} is negative, which shows the reduction in transverse expansion when stress is applied. From elastic constants (C_{11}, C_{12}, C_{44}), we can easily determine the elastic moduli, such as Young's modulus (Y), bulk modulus (B), and shear modulus (G), by using Voigt-Reuss-Hill approximation [54,55].

From elastic constants (C_{11}, C_{12}, C_{44}), we can easily determine the elastic moduli, such as Young's modulus (Y), bulk modulus (B), and shear modulus (G), by using Voigt-Reuss-Hill approximation.

$$B = \frac{1}{3}(C_{11} + 2C_{12}) \tag{4.6.1}$$

$$Y = \frac{9BG_v}{3B+G_v} \tag{4.6.2}$$

$$G = \frac{1}{2}(G_v + G_R) \tag{4.6.3}$$

Where, G_V and G_R are the Voigt shear modulus and Reuss shear modulus, respectively, and are determined by using the following relation [54].

$$G_v = \frac{1}{5}(C_{11} - C_{12} + 3C_{44}) \tag{4.6.4}$$

$$G_R = \frac{5C_{44}(C_{11}-C_{12})}{3(C_{11}-C_{12})+4C_{44}} \tag{4.6.5}$$

Bulk modulus is used to calculate the resistance to volume changes under pressure [56] and maybe simply computed using elastic constants from Equation (4.6.1). Furthermore, Young's modulus (Y) is used to predict a material's stiffness whereas shear modulus (G) is a proportion of resistance to reversible deformation under shear stress that helps to define a material's hardness more precisely than the bulk modulus. Pugh's ratio (B/G) is used to determine a material's brittleness or ductility [54]. If the B/G ratio is more than 1.75, the compound is ductile; otherwise, it is brittle. As a result, both compounds are ductile in our circumstances [56]. All the calculated elastic moduli are listed in Table 4.4.

Table 4.4 Calculated elastic constants, C_{11}, C_{12} and C_{44} (in GPa) and Bulk modulus B(GPa), Young modulus Y(GPa), Shear modulus G(GPa), Poisson's ratio(v), Cauchy pressure ($C_p = C_{12} - C_{44}$) (GPa), Pugh's ratio (B/G) for $NaMCl_3$ (M = In, Al) at zero pressure.

Compounds	C_{11}	C_{12}	C_{44}	B	Y	G	v	C_p	B/G
$NaInCl_3$	48.37	14.89	6.21	26.05	25.07	9.36	0.34	8.68	2.78
$NaAlCl_3$	50.99	16.72	9.20	28.14	31.14	11.84	0.31	7.51	2.37

Thermo dynamical parameters and Debye temperature (θ_D), which are used to depict thermal expansion, melting point, and specific heat capacity, are also associated with mechanical qualities of a material [57]. Debye temperature is connected to the natural frequency of the elastic lattice vibrations and can be determined by averaged elastic-wave velocity (v_m) as

$$\theta_D = \frac{h}{k}\left[\frac{3n}{4\pi}\left(\frac{N_A\rho}{M}\right)\right]^{\frac{1}{3}} v_m \qquad (4.6.6)$$

Here, n is the number of atoms in the molecule, N_A is Avogadro number, and M is the molecular weight. Average sound velocity v_m can also be explained in terms of transverse and longitudinal wave velocities by using the following relation [57,58].

$$v_m = \left[\frac{1}{3}\left(\frac{2}{v_l^3} + \frac{1}{v_t^3}\right)\right]^{-\frac{1}{3}} \qquad (4.6.7)$$

Furthermore, transverse wave velocity v_t and longitudinal wave velocity v_l can be determined by using G and B values as $v_t = \left[\frac{G}{\rho}\right]^{\frac{1}{2}}$ and $v_l = \left[\frac{3B/4G}{\rho}\right]^{\frac{1}{2}}$, respectively [59]. The calculated Debye temperature along with v_m, v_l, and v_t are shown in Table 4.5.

Another essential thermodynamic component, the melting temperature, has been found for these perovskites using Equation (4.6.8) and is given in Table 4.5 based on the data of elastic constants [60].

$$T_m = [553(K) + (5.911)C_{12}]GPa \pm 300K \quad (4.6.8)$$

Table 4.5 Calculated longitudinal (v_l), transverse (v_t) and average (v_m) wave velocities; Debye temperature (θ_D); and melting temperature (T_m) for $NaMCl_3$ (M = In, Al) at zero pressure.

Compounds	v_l(m/s)	v_t(m/s)	v_m(m/s)	θ_D(K)	T_m(K)
$NaInCl_3$	3871.58	1907.97	2142.18	201.847	838.9015±300
$NaAlCl_3$	4656.85	2417.45	2705.62	273.191	854.3568±300

From Table 4.4 and Table 4.5 we can say that our studied materials are metallic. Between $NaMCl_3$ (M = In, Al) compounds $NaAlCl_3$ is more metallic than $NaInCl_3$ because $NaAlCl_3$ have higher melting temperature, higher velocity, higher Debye temperature and higher value of moduli than $NaInCl_3$.

Chapter 5

Conclusion

In this report, the maximum precision full-potential linearized augmented plane wave (FP-LAPW) approach as implemented in the WIEN2k code is used to do density functional studies for compounds $NaMCl_3$ (M = In, Al). The Perdew-Burke-Ernzerhof Generalized-Gradient-Approximation and correlation potential were used to perform detailed behavior analysis on the studied compounds, including structural optimization, band structure, the density of states, real and imaginary dielectric tensor, optical absorption, optical conductivity, reflectivity, refractivity spectra, electron energy loss elastic properties. Structural properties demonstrated that these compounds are cubic and have lattice constants of 5.4030 Å for $NaInCl_3$ and 5.0420 Å for $NaAlCl_3$. Similarly, electronic properties revealed that studied compounds are good metallic conductors that have no band gap. The Density of States also revealed the metallic nature of these compounds. The absorption coefficient, conductivity, and reflectivity showed that our studied compounds are metallic in properties. Elastic properties demonstrated that these compounds have a high melting temperature, high transverse, and longitudinal wave velocities. From Pugh's ratio, we can say that these metals are ductile. So from the above properties, we can conclude that our studied compounds $NaMCl_3$ (M = In, Al) are good conductors and suitable for electrical wires.

Bibliography

[1] Ayaz U, Shazia, Abdullah, et al. Ab initio investigation of structural, electronic, magnetic, elastic, and optical properties of Cs-based chloro-perovskites CsXCl3 (X = Be and Rh). AIP Adv [Internet]. 2021;11:1ENG. Available from: https://doi.org/10.1063/5.0065663.

[2] Reshmi Varma PC. Chapter 7 - Low-Dimensional Perovskites. In: Thomas S, Thankappan ABT-PP, editors. Academic Press; 2018. p. 197–229. Available from: https://www.sciencedirect.com/science/article/pii/B9780128129159000071.

[3] Ayaz U, Shazia, Abdullah, et al. Ab initio investigation of structural, electronic, magnetic, elastic, and optical properties of Cs-based chloro-perovskites CsXCl3 (X = Be and Rh). AIP Adv [Internet]. 2021;11:105215. Available from: https://doi.org/10.1063/5.0065663.

[4] Chi EO, Kim WS, Hur NH. Nearly zero temperature coefficient of resistivity in antiperovskite compound CuNMn3. Solid State Commun [Internet]. 2001;120:307–310. Available from: https://www.sciencedirect.com/science/article/pii/S0038109801003957.

[5] Kim WS, Chi EO, Kim JC, et al. Close correlation among lattice, spin, and charge in the manganese-based antiperovskite material. Solid State Commun. 2001;119:507–510.

[6] Khan K, Sahariya J, Soni A. Structural, electronic and optical modeling of perovskite solar materials ASnX3 (A = Rb, K; X = Cl, Br): First principle investigations. Mater Chem Phys [Internet]. 2021;262:124284. Available from: https://doi.org/10.1016/j.matchemphys.2021.124284.

[7] Lee TD, Ebong AU. A review of thin film solar cell technologies and challenges. Renew Sustain Energy Rev [Internet]. 2017;70:1286–1297. Available from: https://www.sciencedirect.com/science/article/pii/S136403211631070X.

[8] Kannan N, Vakeesan D. Solar energy for future world: - A review. Renew Sustain Energy Rev. 2016;62:1092–1105.

[9] Terki R, Faraoun HI, Bertrand G, et al. Full potential calculation of structural, elastic and electronic properties of BaZrO3 and SrZrO3. Phys status solidi. 2005;242:1054–1062.

[10] Benkabou MH, Harmel M, Haddou A, et al. Structural, electronic, optical and thermodynamic investigations of NaXF3 (X = Ca and Sr): First-principles calculations. Chinese J Phys [Internet]. 2018;56:131–144. Available from: https://doi.org/10.1016/j.cjph.2017.12.008.

[11] C JMD, V M. Coey_Adv_Phys.Pdf. 1999;

[12] Arar R, Ouahrani T, Varshney D, et al. Structural, mechanical and electronic properties of sodium based fluoroperovskites NaXF3 (X=Mg, Zn) from first-principle calculations. Mater Sci Semicond Process. 2015;33:127–135.

[13] Zhao K, Guo Y, Wang Q. Contact properties of a vdW heterostructure composed of penta-graphene and penta-BN2 sheets. J Appl Phys [Internet]. 2018;124:165103. Available from: https://doi.org/10.1063/1.5047539.

[14] Blaha P, Schwarz K, Tran F, et al. WIEN2k: An APW+lo program for calculating the properties of solids. J Chem Phys [Internet]. 2020;152:74101. Available from: https://doi.org/10.1063/1.5143061.

[15] Kohn W, Sham LJ. Self-Consistent Equations Including Exchange and Correlation Effects. Phys Rev [Internet]. 1965;140:A1133--A1138. Available from: https://link.aps.org/doi/10.1103/PhysRev.140.A1133.

[16] Perdew JP, Burke K, Ernzerhof M. Generalized Gradient Approximation Made Simple. Phys Rev Lett [Internet]. 1996;77:3865–3868. Available from: https://link.aps.org/doi/10.1103/PhysRevLett.77.3865.

[17] Schrödinger E. An Undulatory Theory of the Mechanics of Atoms and Molecules. Phys Rev [Internet]. 1926;28:1049–1070. Available from:

https://link.aps.org/doi/10.1103/PhysRev.28.1049.

[18] Sigrist M, Cummings B, Gruyter D, et al. Inhaltsverzeichnis. 2003;13:1–113.

[19] de Wit B, Hoppe J, Nicolai H. On the quantum mechanics of supermembranes. Nucl Physics, Sect B. 1988;305:545–581.

[20] Benenti G, Casati G, Rossini D, et al. Introduction to quantum mechanics. Princ. Quantum Comput. Inf. 2018. p. 55–96.

[21] Koch W, Holthausen MC. A Chemist's Guide to Density Functional Theory. 2000.

[22] Pauli W. The Connection Between Spin and Statistics. Phys Rev [Internet]. 1940;58:716–722. Available from: https://link.aps.org/doi/10.1103/PhysRev.58.716.

[23] Jabs A. Connecting Spin and Statistics in Quantum Mechanics. Found Phys [Internet]. 2010;40:776–792. Available from: https://doi.org/10.1007/s10701-009-9351-4.

[24] Isyaku AO. Structural, Electronic and Optical Properties of Cu 2 Sns 3 Solar Absorber: A First-Principle Density Functional Theory Investigation. 2019; Available from: http://repository.aust.edu.ng/xmlui/handle/123456789/4937.

[25] Zinola CF. Density functional theory. Electrocatal Comput Exp Ind Asp. 2010;117–138.

[26] Dirac PAM. A new notation for quantum mechanics. Math Proc Cambridge Philos Soc. 1939;35:416–418.

[27] Lang C, Pucker N. Mathematische Methoden in der Physik [Internet]. Springer Berlin Heidelberg; 2005. Available from: https://books.google.de/books?id=gXqrAAAACAAJ.

[28] Szabo A, Ostlund NS. Modern Quantum Chemistry: Introduction to Advanced Electronic Structure Theory [Internet]. Dover Publications; 1996. Available from: https://books.google.com.bd/books?id=6mV9gYzEkgIC.

[29] Kohn W. Nobel Lecture: Electronic structure of matter---wave functions and density functionals. Rev Mod Phys [Internet]. 1999;71:1253–1266. Available from: https://link.aps.org/doi/10.1103/RevModPhys.71.1253.

[30] Löwdin P-O. Scaling problem, virial theorem, and connected relations in quantum mechanics. J Mol Spectrosc. 1959;3:46–66.

[31] Hohenberg P, Kohn W. Inhomogeneous Electron Gas. Phys Rev [Internet]. 1964;136:B864--B871. Available from: https://link.aps.org/doi/10.1103/PhysRev.136.B864.

[32] Lei Cheng. First-Principles Density Functional Theory Studies of Reactivities of Heterogeneous Catalysts Determined By Structure and. PHD thesis,BS, Qingdao Univ China [Internet]. 2009;99. Available from: http://opensiuc.lib.siu.edu/dissertations Recommended.

[33] Teller E. On the Stability of Molecules in the Thomas-Fermi Theory. Rev Mod Phys [Internet]. 1962;34:627–631. Available from: https://link.aps.org/doi/10.1103/RevModPhys.34.627.

[34] Balàzs NL. Formation of Stable Molecules within the Statistical Theory of Atoms. Phys Rev [Internet]. 1967;156:42–47. Available from: https://link.aps.org/doi/10.1103/PhysRev.156.42.

[35] Fock V. Näherungsmethode zur Lösung des quantenmechanischen Mehrkörperproblems. Zeitschrift für Phys [Internet]. 1930;61:126–148. Available from: https://doi.org/10.1007/BF01340294.

[36] Hartree DR. The Wave Mechanics of an Atom with a Non-Coulomb Central Field. Part I. Theory and Methods. Math Proc Cambridge Philos Soc. 1928;24:89–110.

[37] Cottenier S. Density Functional Theory and the Family of (L)APW-methods: a step-by-step introduction. Comput. Phys. Reports. 2013.

[38] Martin RM. Electronic: Basic Theory and Practical Methods. 2004;648s.

[39] Ren Y, Hu Y, Hu Z, et al. First-principles study on electronic and optical properties of Zn-substituted CuGaSe2. Results Phys. 2021.

[40] Ceperley DM, Alder BJ. Ground State of the Electron Gas by a Stochastic Method. Phys Rev Lett [Internet]. 1980;45:566–569. Available from: https://link.aps.org/doi/10.1103/PhysRevLett.45.566.

[41] Perdew JP, Zunger A. Self-interaction correction to density-functional approximations for many-electron systems. Phys Rev B [Internet]. 1981;23:5048–5079. Available from: https://link.aps.org/doi/10.1103/PhysRevB.23.5048.

[42] Vosko S ~H., Wilk L, Nusair M. Accurate spin-dependent electron liquid correlation energies for local spin density calculations: a critical analysis. Can J Phys. 1980;59:1200.

[43] Becke AD. Density-functional thermochemistry. II. The effect of the Perdew–Wang generalized-gradient correlation correction. J Chem Phys [Internet]. 1992;97:9173–9177. Available from: https://doi.org/10.1063/1.463343.

[44] Perdew JP, Chevary JA, Vosko SH, et al. Erratum: Atoms, molecules, solids, and surfaces: Applications of the generalized gradient approximation for exchange and correlation. Phys Rev B [Internet]. 1993;48:4978. Available from: https://link.aps.org/doi/10.1103/PhysRevB.48.4978.2.

[45] Kokalj A. Computer graphics and graphical user interfaces as tools in simulations of matter at the atomic scale. Comput Mater Sci [Internet]. 2003;28:155–168. Available from: https://www.sciencedirect.com/science/article/pii/S0927025603001046.

[46] Canadell E, Doublet M-L, Iung C. Density of states. 2012.

[47] Wang J, Wang Z, Jing Y, et al. Electronic structure and optical properties of boron suboxide B6O system: First-principles investigations. Solid State Commun. 2016;244:12–16.

[48] Dar SA, Srivastava V, Sakalle UK. A combined {DFT} and post-{DFT} investigation on cubic {XMoO}3(X{\hspace{0.167em}}{\hspace{0.167em}}={\hspace{0.167em}}{\hspace{0.167em}}Sr, Ba) perovskite oxides. Mater Res Express [Internet]. 2017;4:86304. Available from: https://doi.org/10.1088/2053-1591/aa84a6.

[49] Dar SA, Srivastava V, Sakalle UK, et al. Ferromagnetic Phase Stability, Magnetic, Electronic, Elasto-Mechanical and Thermodynamic Properties of BaCmO3 Perovskite Oxide. J Electron Mater [Internet]. 2018;47:3809–3816. Available from: https://doi.org/10.1007/s11664-018-6251-4.

[50] Mouhat F, Coudert F \mbox\cc\else ç\fiois-X. Necessary and sufficient elastic stability conditions in various crystal systems. Phys Rev B [Internet]. 2014;90:224104. Available from: https://link.aps.org/doi/10.1103/PhysRevB.90.224104.

[51] Born M. On the stability of crystal lattices. I. Math Proc Cambridge Philos Soc.

1940;36:160–172.

[52] Kong Y, Duan YH, Li LMR. Phase stability, elastic anisotropy and electronic structure of cubic MAl2 (M=Mg, Ca, Sr and Ba) Laves phases from first-principles calculations. Mater Res Express. 2016;3.

[53] Deligoz E, Ozisik H. Mechanical and dynamical stability of TiAsTe compound from ab initio calculations. Philos Mag. 2015;95.

[54] Iftikhar A, Ahmad A, Ahmad I, et al. DFT study on thermo-elastic properties of Ru2FeZ (Z = Si, Ge, Sn) Heusler alloys. Int J Mod Phys B [Internet]. 2017;32:1850045. Available from: https://doi.org/10.1142/S0217979218500455.

[55] Hill R. The Elastic Behaviour of a Crystalline Aggregate. Proc Phys Soc Sect A [Internet]. 1952;65:349–354. Available from: http://dx.doi.org/10.1088/0370-1298/65/5/307.

[56] Pugh SF. XCII. Relations between the elastic moduli and the plastic properties of polycrystalline pure metals. London, Edinburgh, Dublin Philos Mag J Sci [Internet]. 1954;45:823–843. Available from: https://doi.org/10.1080/14786440808520496.

[57] Miao N, Sa B, Zhou J, et al. Theoretical investigation on the transition-metal borides with Ta3B4-type structure: A class of hard and refractory materials. Comput Mater Sci. 2011;50:1559–1566.

[58] Riley WF. Book Reviews : ELASTIC CONSTANTS AND THEIR MEASUREMENT E. Schreiber, O. L. Anderson, and N. Soga McGraw-Hill Book Co., New York, N. Y. (1973). Shock Vib Dig. 1975;7:120.

[59] Bakhshayeshi A, Sarmazdeh M, Mendi R, et al. First-Principles Prediction of Electronic, Magnetic, and Optical Properties of Co2MnAs Full-Heusler Half-Metallic Compound. J Electron Mater. 2016;46.

[60] Dar A, Srivastava V, Sakalle U. Ab-initio DFT based investigation of double perovskite oxide Ba2CdOsO6 with cubic structure. Comput Condens Matter. 2018;18:e00351.